Article

Cell Reports

Molecularly Distinct Clathrin-Coated Pits Differentially Impact EGFR Fate and Signaling

Graphical Abstract

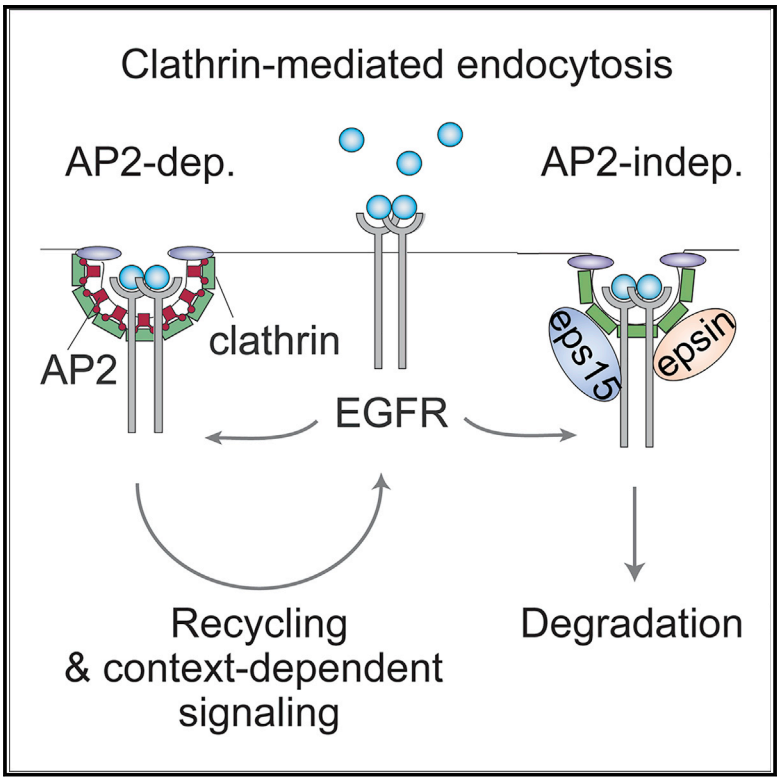

Authors

Roberta Pascolutti, Veronica Algisi, Alexia Conte, ..., Tom Kirchhausen, Pier Paolo Di Fiore, Sara Sigismund

Correspondence

sara.sigismund@ieo.it

In Brief

EGFR signaling controls different cell physiological processes, including proliferation and migration. Pascolutti et al. describe an additional layer of regulation of EGFR signaling, relying on the sequestration of receptors into molecularly distinct clathrin-coated vesicles that regulate receptor fate toward recycling versus degradation, with impact on the final cellular output.

Highlights

- Distinct classes of CCPs exist, molecularly defined by the presence or lack of AP2
- The AP2-negative CCPs support the internalization of EGFR but not of TfR
- The AP2-negative CCPs rely on the endocytic adaptors eps15/eps15L1 and epsin1
- The two classes of CCPs determine distinct EGFR fates and signaling outputs

Pascolutti et al., 2019, Cell Reports *27*, 3049–3061
June 4, 2019
https://doi.org/10.1016/j.celrep.2019.05.017

CellPress

Cell Reports
Article

Molecularly Distinct Clathrin-Coated Pits Differentially Impact EGFR Fate and Signaling

Roberta Pascolutti,[1,12,14] Veronica Algisi,[1,13,14] Alexia Conte,[1,2] Andrea Raimondi,[3] Mithun Pasham,[4] Srigokul Upadhyayula,[4,5,6] Raphael Gaudin,[4,7,11] Tanja Maritzen,[8] Elisa Barbieri,[1,2] Giusi Caldieri,[1,2,9] Chiara Tordonato,[2] Stefano Confalonieri,[1,2] Stefano Freddi,[2] Maria Grazia Malabarba,[1,2,9] Elena Maspero,[1] Simona Polo,[1,9] Carlo Tacchetti,[3,10] Volker Haucke,[8] Tom Kirchhausen,[4,5,6,7] Pier Paolo Di Fiore,[1,2,9] and Sara Sigismund[1,2,9,15,*]

[1]IFOM, Fondazione Istituto FIRC di Oncologia Molecolare, Via Adamello 16, 20139 Milan, Italy
[2]Istituto Europeo di Oncologia IRCCS, Via Ripamonti 435, 20141 Milan, Italy
[3]Experimental Imaging Centre, Istituto di Ricovero e Cura a Carattere Scientifico (IRCCS), San Raffaele Scientific Institute, via Olgettina 58, 20132 Milan, Italy
[4]Program in Cellular and Molecular Medicine, Boston Children's Hospital, Boston, MA 02115, USA
[5]Department of Pediatrics, Harvard Medical School, Boston, MA 02115, USA
[6]Janelia Research Campus, Howard Hughes Medical Institute, Ashburn, VA 20147, USA
[7]Department of Cell Biology, Harvard Medical School, Boston, MA 02115, USA
[8]Leibniz-Forschungsinstitut für Molekulare Pharmakologie (FMP), Robert-Roessle-Straße 10, 13125 Berlin, Germany
[9]Università degli Studi di Milano, Dipartimento di Oncologia ed Emato-oncologia, Via Santa Sofia 9/1, 20122 Milan, Italy
[10]Università Vita-Salute San Raffaele, Milan, Italy
[11]Institut de Recherche en Infectiologie de Montpellier, UMR 9004, CNRS/UM, 1919 route de Mende, 34293 Montpellier cedex 5, France
[12]Present address: Department of Biological Chemistry and Molecular Pharmacology, Harvard Medical School, Boston, MA 02115, USA
[13]Present address: Syneos Health, Clinical Department, Via M. Gonzaga 7, 20123 Milan, Italy
[14]These authors contributed equally
[15]Lead Contact
*Correspondence: sara.sigismund@ieo.it
https://doi.org/10.1016/j.celrep.2019.05.017

SUMMARY

Adaptor protein 2 (AP2) is a major constituent of clathrin-coated pits (CCPs). Whether it is essential for all forms of clathrin-mediated endocytosis (CME) in mammalian cells is an open issue. Here, we demonstrate, by live TIRF microscopy, the existence of a subclass of relatively short-lived CCPs lacking AP2 under physiological, unperturbed conditions. This subclass is retained in AP2-knockout cells and is able to support the internalization of epidermal growth factor receptor (EGFR) but not of transferrin receptor (TfR). The AP2-independent internalization mechanism relies on the endocytic adaptors eps15, eps15L1, and epsin1. The absence of AP2 impairs the recycling of the EGFR to the cell surface, thereby augmenting its degradation. Accordingly, under conditions of AP2 ablation, we detected dampening of EGFR-dependent AKT signaling and cell migration, arguing that distinct classes of CCPs could provide specialized functions in regulating EGFR recycling and signaling.

INTRODUCTION

Clathrin-mediated endocytosis (CME) is the best-characterized route of internalization for plasma membrane (PM)-resident proteins, thereby regulating a variety of cellular functions ranging from metabolism to signaling and neurotransmission (Robinson, 2015; Kirchhausen et al., 2014). In mammalian cells, adaptor protein 2 (AP2) is the most abundant clathrin adaptor, involved in the early phase of clathrin-coated pit (CCP) nucleation and maturation (Robinson, 2015; Kirchhausen et al., 2014; McMahon and Boucrot, 2011). As CCPs gain curvature and mature, AP2 recruits cargoes. This step represents an "endocytic checkpoint," as failure to recruit cargo results in short-lived, abortive CCPs (Kadlecova et al., 2017; Kelly et al., 2014; Aguet et al., 2013; Carroll et al., 2012; Henry et al., 2012; Liu et al., 2010; Loerke et al., 2009; Puthenveedu and von Zastrow, 2006; Ehrlich et al., 2004). Fission of cargo-loaded, deeply invaginated CCPs is executed by the GTPase dynamin, leading to the release of clathrin-coated vesicles (CCVs) (for a review see Antonny et al., 2016). Although clathrin, AP2, dynamin, and cargo constitute the basic components of a CCP, a variety of accessory proteins have been implicated in the assembly and in the maturation of CCPs (Kaksonen and Roux, 2018; Kirchhausen et al., 2014; Merrifield and Kaksonen, 2014; Mettlen et al., 2009).

AP2 is highly conserved from yeast to human (Schledzewski et al., 1999; Nakayama et al., 1991; Kirchhausen, 1990). Notably, it is not essential for viability or for CME in yeast, and other adaptors can substitute for it (Lu et al., 2016; Brach et al., 2014; Weinberg and Drubin, 2012). Moreover, differently from mammalian cells, CCP nucleation in yeast does not require AP2 binding motifs in the cargo cytosolic tail (e.g., Yxxφ), while ubiquitination of cargo and adaptors is critical (Weinberg and Drubin, 2012, 2014). In contrast, AP2 is indispensable for embryonic development of *Drosophila*, *C. elegans*, and mice (Gu et al., 2008; Mitsunari et al., 2005; González-Gaitán and Jäckle, 1997), and it is thought to be essential for CCP nucleation in mammalian cells (Cocucci et al., 2012). Most studies in mammalian cells have

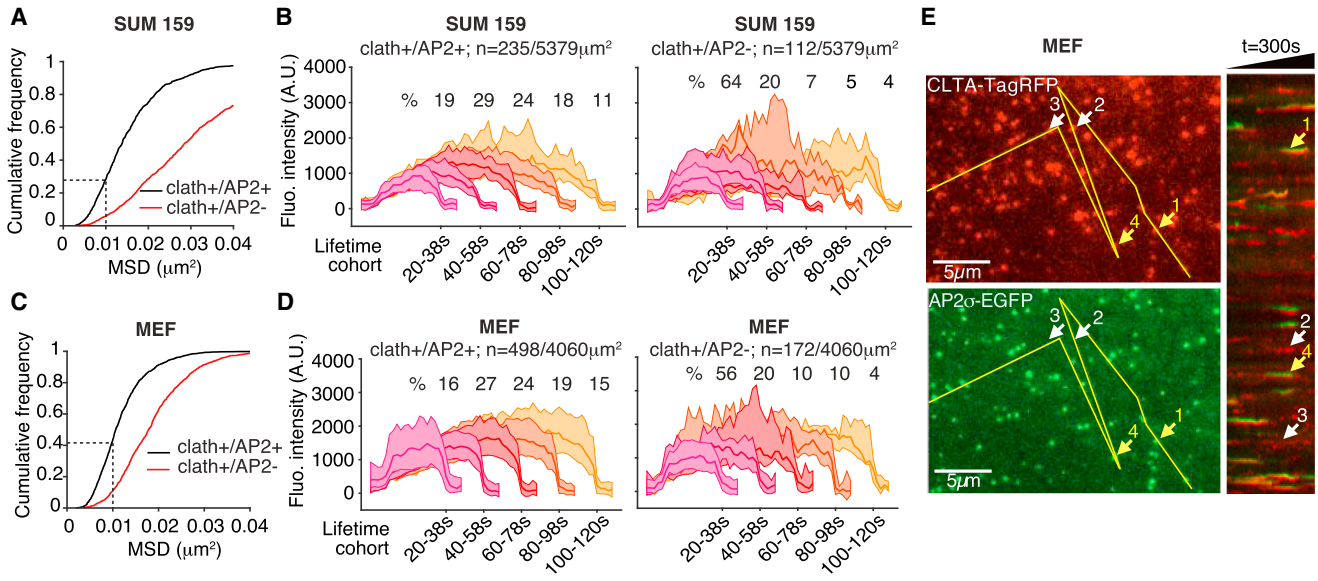

Figure 1. Live TIRF Imaging of CCPs in SUM159 and AP2-WT MEF Cells

(A) Cumulative frequency distribution of the initial mean square displacement (MSD) of clathrin-coated structures containing or not AP2 in SUM159 cells imaged by TIRF. Clathrin events with initial MSD larger than 0.01 μm^2 (dotted line) were excluded from the plots displaying fluorescence intensity cohorts (B).

(B) Automated analysis of clathrin-coated structure formation at the plasma membrane of SUM159 cells obtained from 13 cells and ~350 clathrin traces. The analysis for traces excluding events with lifetimes < 20 s shows average fluorescence intensity plots (mean ± SD) grouped as cohorts according to their lifetimes. The left panel corresponds to 235 events containing CLTA-TagRFP and AP2-σ2-EGFP (clathrin+/AP2+), while the right panel corresponds to 112 events devoid of AP2-σ2-EGFP (clathrin+/AP2−).

(C) Cumulative frequency distribution of the initial MSD of clathrin-coated structures containing or not AP2 in MEF AP2-WT cells imaged by TIRF. Clathrin events with initial MSD larger than 0.01 μm^2 (dotted line) were excluded in the plots displaying fluorescence intensity cohorts (D).

(D) Automated analysis of clathrin-coated structure formation at the plasma membrane from 8 cells and ~670 clathrin traces from MEF WT cells.

(E) Representative TIRF microscopy time series acquired every 2 s from the bottom surface of MEF cells, stably expressing clathrin light chain A tagged with TagRFP (CLTA-TagRFP) together with σ2 of AP2 tagged with EGFP (AP2σ-EGFP). The TIRF snapshots (left) were recorded at 224 and 138 s, and the corresponding right panels are kymographs from the complete time series. The yellow tracings display the path used to generate the kymographs. The green channels in the kymographs were shifted upward by 5 pixels. The majority of the endocytic clathrin structures contained clathrin together with AP2 in the WT cells (e.g., pits 1 and 4), and few contained only clathrin (e.g., pits 2 and 3).

focused on constitutive endocytosis (see, e.g., Aguet et al., 2013; Cocucci et al., 2012; Loerke et al., 2009), mainly using transferrin receptor (TfR) as model cargo, for which AP2 appears to be essential (Boucrot et al., 2010; Liu et al., 2010; Mettlen et al., 2009; Huang et al., 2004; Hinrichsen et al., 2003; Motley et al., 2003). In contrast, ligand-induced receptor internalization might occur in the absence of AP2, as AP2 knockdown (KD) experiments have shown that the internalization of some signaling receptors can still occur under conditions of functional AP2 ablation (Johannessen et al., 2006; Maurer and Cooper, 2006; Huang et al., 2004; Hinrichsen et al., 2003; Motley et al., 2003).

From these latter observations, it appears that AP2-independent mechanisms of CME also exist in mammalian cells. The issue, however, is debated and far from being settled for two main reasons: (1) it cannot be excluded that residual levels of AP2 in the KD experiments are indeed responsible for the residual CME, and (2) under unperturbed conditions, no conclusive imaging-based evidence has been produced showing that a significant fraction of clathrin-dependent internalization events occur in the absence of AP2 in the forming pit.

The issue is of particular relevance for those signaling receptors, such as epidermal growth factor receptor (EGFR), which might be internalized via AP2-dependent and AP2-independent CME (Huang et al., 2004; Hinrichsen et al., 2003; Motley et al., 2003), also considering the large variety of endocytic factors and internalization and sorting signals involved in EGFR endocytosis (Goh et al., 2010). These considerations highlight a number of unresolved questions. (1) Do different modalities of CME exist under physiological conditions? (2) Are they cargo selective? (3) Are they differentially coupled to receptor fate and/or signaling? The present studies were undertaken to address these questions.

RESULTS

A Subclass of Short-Lived CCPs Lacking AP2

To investigate whether different subclasses of clathrin-coated structures (CCSs), characterized by the presence versus absence of AP2, exist under physiological conditions, we used SUM159 cells that were gene-edited to express AP2σ2-EGFP and CLTA-TagRFP (see STAR Methods). We monitored CCS dynamics by live total internal reflection fluorescence (TIRF) microscopy as previously described (Aguet et al., 2013; Cocucci et al., 2012). In this analysis, we adopted a rather stringent cutoff by excluding events that were highly motile with an initial mean square displacement (MSD) larger than 0.01 μm^2 (Figure 1A). This was done to minimize the contribution of CCVs originating from the

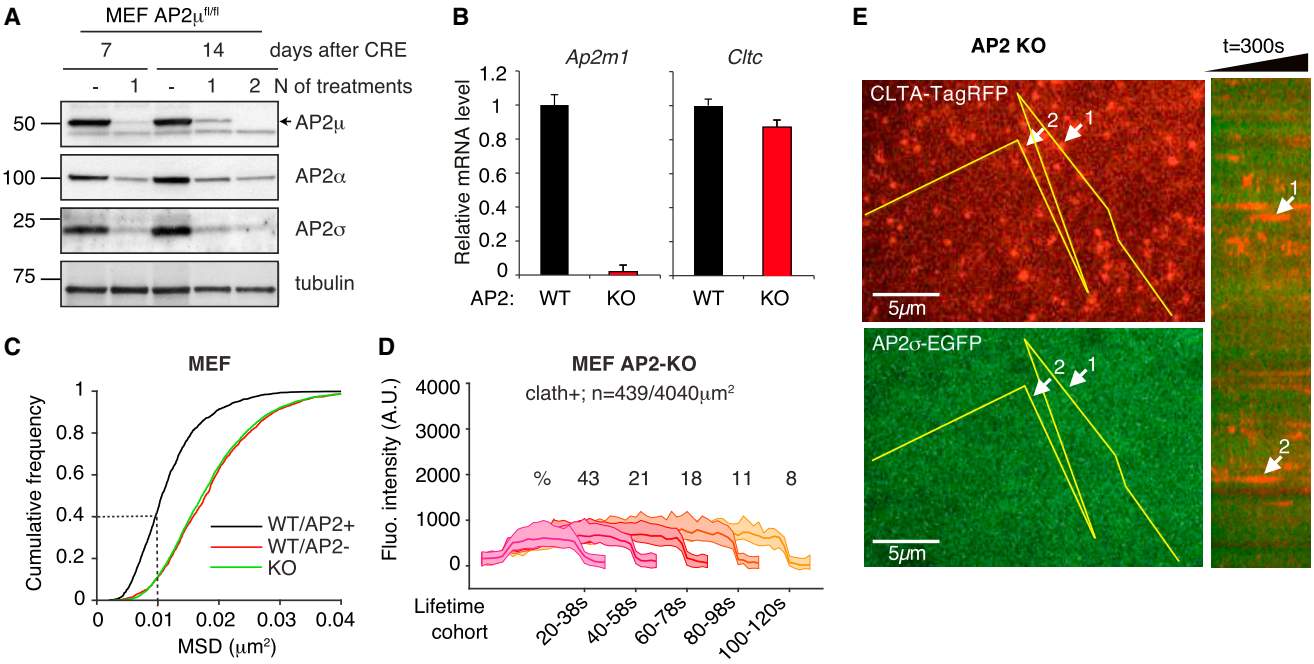

Figure 2. Live TIRF Imaging of CCPs in AP2 KO MEF Cells

(A) MEFs from conditional AP2$\mu^{fl/fl}$ mice (Figure S2A) were treated *in vitro* with CRE recombinase, as indicated, followed by immunoblotting (IB) as shown. The lower band in the AP2μ IB is nonspecific; the specific AP2μ band is indicated by an arrow. In all subsequent experiments, AP2$\mu^{fl/fl}$ MEFs were either left untreated or treated with CRE for 14 days-two rounds (henceforth referred as AP2-WT and AP2-KO, respectively).

(B) AP2-WT and AP2-KO MEFs were analyzed for mRNA levels of *Ap2m1* and *Cltc* using qRT-PCR. mRNA levels are reported relative to untreated controls and normalized to the *18S* gene. Error bars are calculated on technical replicates (n = 3).

(C) Cumulative frequency distribution of the initial MSD of clathrin-coated structures in MEF AP2-WT and AP2-KO cells imaged by TIRF. Clathrin events with initial MSD larger than 0.01 μm^2 (dotted line) were excluded in the plots displaying fluorescence intensity cohorts (D).

(D) Automated analysis of clathrin-coated structure formation at the plasma membrane from 12 cells and ~439 clathrin traces from MEF KO cells.

(E) Representative TIRF microscopy time series acquired every 2 s from the bottom surface of MEF AP2-KO cells, stably expressing CLTA-TagRFP together with AP2σ-EGFP. The TIRF snapshots (left) were recorded at 224 and 138 s, and the corresponding right panels are kymographs from the complete time series. The yellow tracings display the path used to generate the kymographs. The green channels in the kymographs were shifted upward by 5 pixels. Endocytic "clathrin-only" structures are present (e.g., pits 1 and 2).

secretory pathway. Under these conditions, 30%–40% of all detected events were computed. We found that 55%–70% of these clathrin-positive events (excluding events below 20 s and above 120 s in duration) were also positive for AP2, while the rest lacked the AP2 signal (Figure 1A). All the recorded events, presumably membrane bound and termed here CCPs, were grouped in cohorts with a specific range of lifetimes (Figure 1B). This revealed that although clathrin+/AP2+ events were almost equally distributed in the lifetime cohorts between 20 and 80 s, the clathrin+/AP2− events were enriched in the cohorts with shorter lifetime (20–38 s). This argues for the existence, under physiological conditions, of a subclass of endocytic CCPs lacking AP2, which are generally short lived and smaller than AP2-containing CCPs, while displaying a similar intensity-growth profile and comparable dynamics. Of note, when the MSD threshold for inclusion was raised to 0.0155 or to 0.02 μm^2, results superimposable to those described above were obtained (Figure S1).

Next, used mouse embryonic fibroblasts (MEFs) derived from AP2μ conditional knockout (KO) mice (AP2$\mu^{fl/fl}$, henceforth AP2-WT [wild-type]; Figure S2A; Soykan et al., 2016; Kononenko et al., 2014). These cells were engineered to stably express AP2σ2-EGFP and CLTA-TagRFP as transgenes (see Figures S2B and S2C and their legends for details). In this model, before CRE treatment (AP2-WT cells), we confirmed the phenotypes observed in SUM159 cells; in particular, we could detect about one-third of the clathrin-positive events that lacked the AP2 signal (Figures 1C–1E). Importantly, these events fell mainly in the short-lived cohort of CCPs (Figures 1C–1E; see also Figures S2D and S2E, left and center). In contrast, fewer than 1% of all the AP2-positive events lacked clathrin (clathrin−/AP2+).

Treatment of AP2-WT MEFs with CRE recombinase induced the excision of exons 2 and 3 of the *Ap2m1* gene (henceforth AP2-KO; Figure S2A) and the loss of AP2μ protein expression (Figures 2A and 2B). In AP2-KO MEFs, clathrin-positive events persisted, with frequency and cohort distribution resembling those observed for the AP2-negative CCPs in AP2-WT cells (Figures 2C–2E; see also Figures S2D and S2E, right). These data argue that a subset of CCPs can form also in the complete absence of AP2.

Morphological Analysis of CCPs Formed in AP2-KO MEFs

We performed electron microscopy (EM) of PM sheets prepared from AP2-WT and AP2-KO MEFs. This confirmed that CCSs form in the absence of AP2 (Figure 3A). The surface density of CCS was reduced by ~80% in AP2-KO MEFs versus AP2-WT

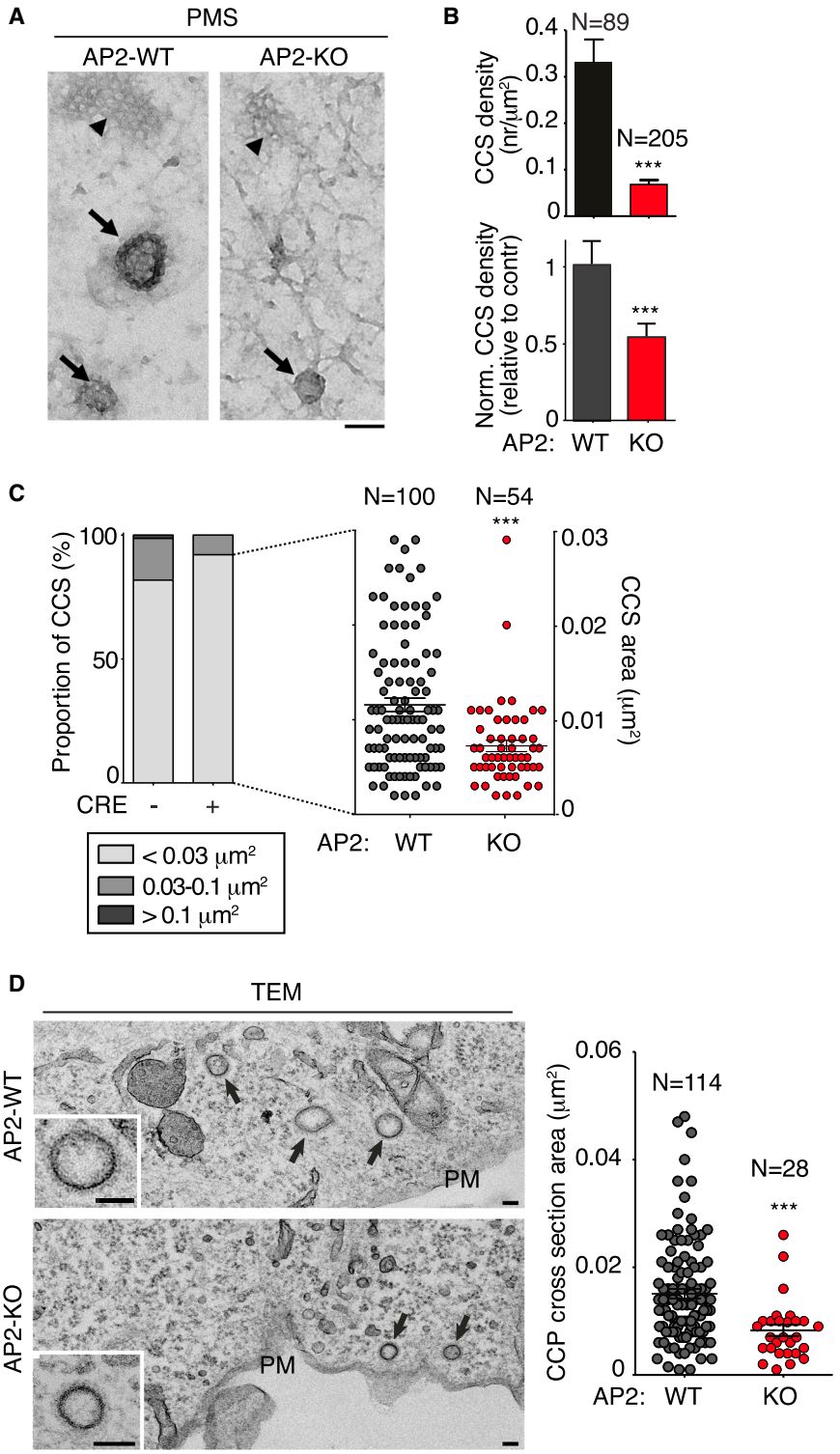

Figure 3. Morphological Characterization of CCPs in AP2-WT and AP2-KO Cells

(A) Plasma membrane sheets (PMSs) of AP2-WT and AP2-KO MEFs showing examples of clathrin-coated structures (arrowheads, flat clathrin lattices; big arrows, CCPs). Bar, 100 nm.

(B) Top: CCS density in AP2-WT and AP2-KO MEFs. Bottom: CCS number was normalized for surface area (Figure S3A; STAR Methods) and expressed relative to control cells. N represents the number of random images analyzed. Data are represented as mean ± SEM. p values were calculated using two-tailed Student's t test (***p < 0.001).

(C) Left: size distribution of CCSs in AP2-WT and AP2-KO MEFs (STAR Methods; Grove et al., 2014). Right: analysis of distribution of CCP areas in AP2-WT and AP2-KO MEFs. Only CCPs < 0.03 μm^2 were included in the analysis. N represents the number of CCSs analyzed. p values were calculated using two-tailed Student's t test (***p < 0.001).

(D) Transmission electron microscopy (TEM) analysis of CCPs in AP2-WT and AP2-KO MEFs. In AP2-KO cells, CCPs appear smaller compared with AP2-WT cells (arrows and insets), as also shown by the morphometric analysis in the right panel. N represents the number of random images analyzed. Bar, 100 nm. p values were calculated using two-tailed Student's t test (***p < 0.001).

(Figure 3B, top). However, the cell surface area of AP2-KO MEFs was greatly enlarged versus AP2-WT (~2.5-fold surface increase; Figure S3A). When normalized for cell surface area, AP2-KO MEFs showed a ~50% decrease in CCSs versus controls (Figure 3B, bottom). Importantly, the disappearance of large and medium CCSs (including flat clathrin lattices and plaques; Grove et al., 2014; Saffarian et al., 2009) and a shift toward smaller structures (≤0.03 μm^2) were observed in AP2-KO MEFs (Figure 3C, left), as also previously shown in AP2-KD HeLa cells (Miller et al., 2015; Motley et al., 2003). Analysis of the area distribution of the CCSs with size ≤ 0.03 μm^2 showed that AP2-KO MEFs had lost larger CCSs, while retaining the smaller ones, with compared to WT cells (Figure 3C, right), as also confirmed by transmission EM (TEM) (Figure 3D and its legend). These data indicated that small CCPs present in WT cells are retained upon AP2 KO.

EGFR-CME Occurs in AP2-KO Cells

The availability of AP2-KO cells afforded the opportunity to test the impact of the bona fide total absence of AP2 on CME of receptors whose internalization proceeds constitutively (exemplified by the TfR) or in a ligand-induced fashion (exemplified by the EGFR).

The measurement of EGFR endocytosis is complicated by the fact that the receptor can be internalized both through CME and

through non-clathrin endocytosis (NCE). CME is active already at low doses (1–3 ng/mL) of ligand and persists at higher doses; NCE, conversely, is activated only at higher doses (≥10 ng/mL; Caldieri et al., 2017; Sigismund et al., 2013). The issue is further compounded by the fact that the presence of the EGFR-NCE pathway is context dependent: some cells (e.g., HeLa cells) possess the pathway whereas others do not (Caldieri et al., 2017; Sigismund et al., 2013). Experimentally this is reflected in a differential impact of clathrin KD on epidermal growth factor (EGF) internalization performed at different doses of the ligand (Sigismund et al., 2013). The MEFs under scrutiny here seem to internalize EGFR exclusively through CME, as witnessed by findings that clathrin KD equally reduced the internalization rate by >85% at both low and high doses of ligand (Figure S3B). Thus, in principle CME-dependent EGFR internalization could be studied in our MEFs at either dose. However, because one of our goals was to compare the AP2-KO setting to the KD settings obtained in different cell lines (in which NCE might be present), all the kinetics internalization experiments with ^{125}I-EGF were performed at low ligand (1.5 ng/mL).

Under these conditions, in AP2-KO cells ^{125}I-EGF internalization rate was reduced by only ~50% versus the WT control and further reduced upon clathrin-KD (Figure 4A, left; Figure S3C). Conversely, ^{125}I-Tf (transferrin) internalization was reduced to background levels (defined as the amount measured in clathrin-KD cells) (Figure 4A, right).

The results in KO MEFs were virtually indistinguishable from those obtained upon AP2-KD in HeLa cells (Figure S3D; Huang et al., 2004; Motley et al., 2003) and in a variety of normal or cancer cell lines of human or murine origin (Figure 4B).

Together these results allow a number of initial conclusions: (1) the differential impact on Tf versus EGF uptake upon AP2 removal was formally proven in a clean genetic KO background; (2) the KD data are reliable because they phenocopy those obtained in the KO system; and (3) the effects of AP2 removal on cargo uptake are indistinguishable under acute (KD) or chronic (KO) conditions, thereby ruling out a number of potential caveats, such as adaptation in the KO conditions or insufficient targeting or off-target effects in the silencing condition.

EM Characterization of AP2-Independent CME

To characterize morphologically the EGFR-internalizing structures in AP2-KO cells, we used TEM. The endogenous levels of expression of the EGFR in MEFs were too low to detect a sufficient number of events for quantitative measurements. We circumvented this problem with a twofold strategy: (1) we increased the expression levels of EGFR using a doxycycline-inducible EGFR expression system; upon doxycycline treatment, we obtained EGFR surface levels in MEFs comparable with those detectable in HeLa cells (see Figure S3E); and (2) we stimulated the cells with high doses of EGF (30 ng/mL) because we showed (Figure S3B) that in these cells, only the CME pathway is active. We found, in agreement with the functional data, that EGFR was still recruited to small CCPs and CCVs in AP2-KO MEFs, as visualized either by pre-embedding gold immunolabeling of the EGFR stimulated with unlabeled EGF (Figure 4C) or by gold labeling with anti-Alexa 488 antibody of cryosections from cells stimulated with Alexa 488-EGF (Figures S3F and S3G; see STAR Methods and Caldieri et al., 2017). EGFR-positive structures were reduced by ~60% versus control cells (Figure 4D, left). Importantly, the number of gold particles per CCP was significantly reduced (Figure 4D, right). Thus, a consequence of reduced CCP size is a reduction in cargo loading, under conditions of AP2 KO.

Alternative Endocytic Adaptors Required for AP2-Independent EGFR-CME

How do EGFR-containing CCPs form in the absence of AP2? We investigated the possibility that other AP complexes might functionally substitute for AP2. This was not the case, as clathrin-dependent internalization kinetics of ^{125}I-EGF in AP2-KO MEFs were unaffected by KD of the different AP complexes (AP1, AP3, AP4, and AP5) (Figures 5A and S4A).

In search of alternative adaptors, we explored the role of known endocytic proteins, eps15, eps15L1, and epsin1, which we have previously shown to have a redundant role in EGFR-CME (Savio et al., 2016; Sigismund et al., 2005). Indeed, although eps15/eps15L1 KD or epsin1 KD in HeLa cells reduced EGFR-CME by ~25%, the triple eps15/eps15L1/epsin1 KD (henceforth triple-KD) resulted in a ~50% decrease in the EGFR internalization rate (Figures 5B, S4B, and S4C). The addition of epsin2 KD did not worsen the phenotype of the double eps15/eps15L1 KD or of the triple eps15/eps15L1/epsin1 KD (see Figures S4B–S4D and their legends). When the triple-KD was combined with AP2-KD, the EGFR internalization rate was decreased to clathrin-KD levels (Figures 5B and S4E). Because these data were confirmed in AP2-KO MEFs subjected to triple-KD (Figures 5C, S4D [bottom], and S4F), we propose that eps15/eps15L1/epsin1 are responsible for the residual EGFR-CME observed in the absence of AP2.

EM analysis of triple-KD MEFs (in the AP2-WT-EGFR background) revealed a decrease in the number of EGFR-positive CCPs versus control cells (Figure 5D, left; Figure S3A), with no apparent defects in CCS size and no reduction in the number of gold particles per CCS (Figure 5D, center and right), suggesting that the ablation of eps15/eps15L1/epsin1 alters CCP formation and/or stability and affects EGFR-CME but not CCP size and cargo loading.

These data were confirmed by live TIRF microscopy, showing that triple-KD cells display a reduced CCP number per square micrometer (~60% of the events compared with WT cells), while showing the same CCP fluorescence intensity and lifetime distribution as WT cells (Figures 5E and S5).

AP2 Is Not Required for EGFR Degradation, but It Is Essential for EGF-Dependent AKT Signaling and Cell Migration

The previous observations suggest that AP2 is not an absolute requirement for EGFR-CME. In its absence, the internalization of the receptor can still proceed, albeit less efficiently, through a mechanism based on the endocytic accessory proteins eps15/eps15L1 and epsin1. Our data also suggest that AP2, directly or indirectly, controls CCP size, as previously reported (Dambournet et al., 2018; Miller et al., 2015), as supported by the observation that CCPs lacking AP2 are smaller and also contain less EGFRs. To test how these function(s) of AP2 might

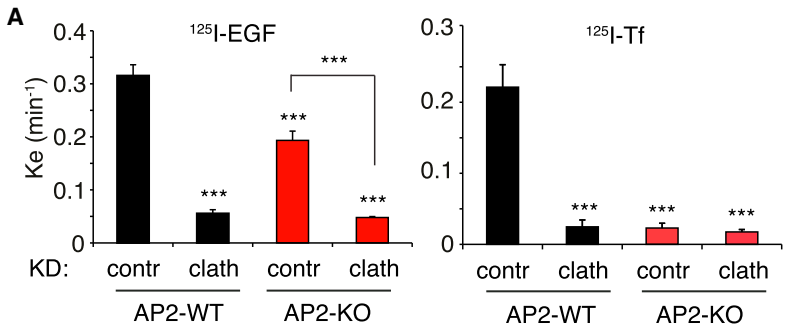

B

Cell Line EGFRs/cell		^{125}I-EGF Ke	AP2-indep. CME (%)
HeLa 2.7 x 10^5	control	0.29	40%
	AP2 KD	0.17	
	clath KD	0.09	
NR6-EGFR 2.5 x 10^5	control	0.20	38%
	AP2 KD	0.10	
	clath KD	0.04	
A431 1.2 x 10^6	control	0.18	33%
	AP2 KD	0.08	
	clath KD	0.03	
MDA MB-231 0.8 x 10^5	control	0.19	53%
	AP2 KD	0.12	
	clath KD	0.04	
MCF10A 2.9 x 10^5	control	0.22	69%
	AP2 KD	0.17	
	clath KD	0.06	
HCT116 0.5 x 10^5	control	0.06	40%
	AP2 KD	0.03	
	clath KD	0.01	

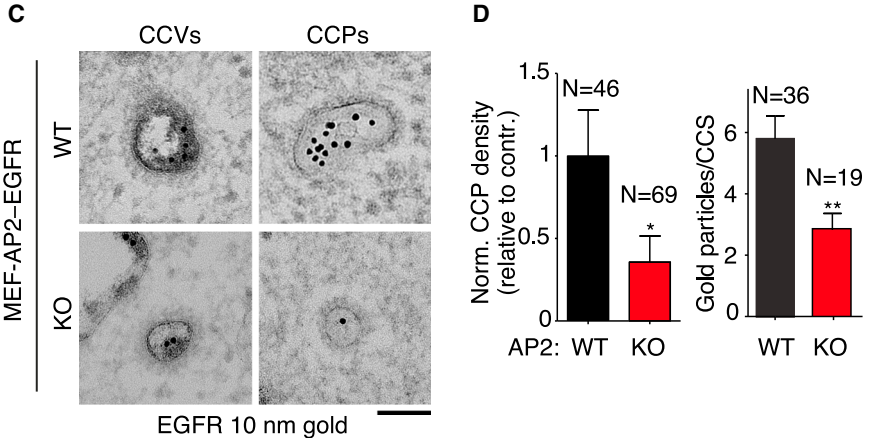

Figure 4. EGF Internalization in AP2-KO MEFs or upon AP2-KD in Different Cell Contexts

(A) ^{125}I-EGF (left) and ^{125}I-Tf (right) internalization in AP2-WT and AP2-KO MEFs in the presence or absence of clathrin KD. Internalization constants (K_e) are the mean ± SD of two independent experiments. p values were calculated using each pair Student's t test (***p < 0.001).

(B) Analysis of the impact of AP2μ KD versus clathrin KD in different cell lines as indicated. The number of EGFRs per cell in the different cell lines was measured using ^{125}I-EGF saturation binding assay. Kinetics of ^{125}I-EGF (1.5 ng/mL) were measured and are reported as internalization constants (K_e). The percentage of AP2-independent EGFR internalization was calculated from the residual K_e in AP2-KD cells relative to the K_e in control cells (after subtracting the residual internalization in clathrin KD cells; Sigismund et al., 2013).

(C) TEM analysis of EGFR internalization. AP2-WT and AP2-KO MEFs expressing EGFR under a doxycycline-inducible promoter (AP2-EGFR) were induced with doxycycline. Cells were then subjected to *in vivo* immunolabeling with anti-EGFR 13A9 antibody and 10 nm protein A-gold, stimulated 5 min with EGF (30 ng/mL), and fixed in the presence of ruthenium red, to distinguish PM-connected CCPs (ruthenium red positive) and internalized CCVs (ruthenium red negative) structures. Bar, 100 nm.

(D) Morphometrical analysis of (C). Left: CCP number was normalized for the difference in PM length between AP2-KO MEFs versus control (~1.5-fold increase; see Figure S3A and STAR Methods) and expressed as relative to control cells. Right: number of gold particles per CCS (CCPs + CCVs). N represents the numbers of random images (left) and CCSs (right) analyzed. Data are expressed as mean ± SEM. p values were calculated using two-tailed Student's t test (*p < 0.05 and **p < 0.01).

affect EGF-dependent cellular phenotypes, we performed the following experiments.

First, we investigated the fate of the EGFR after CME in control HeLa cells or upon AP2-KD. To avoid the combined occurrence of EGFR-CME and EGFR-NCE, we used low EGF doses. At low EGF dose in HeLa cells, the EGF-bound receptors internalized via CME are either recycled (about 70%) or targeted to degradation (30%; Sigismund et al., 2008). However, at low non-saturating EGF concentrations, only a minor fraction of EGFRs are engaged by the ligand; hence, the degradation of that fraction over the total EGFR pool is not readily detectable by immunoblotting, but it could be easily detected by following degradation (and recycling) of the iodinated ligand, which provides accurate quantitative measurements and can be used as a proxy for receptor degradation (Pinilla-Macua and Sorkin, 2015; Sigismund et al., 2008; Sorkin et al., 1991). With this assay, we found that in AP2-depleted HeLa cells, despite reduced EGFR-CME, the degradation of the internalized ligand proceeded at a sustained pace and was actually higher than in WT cells, possibly as a consequence of reduced recycling

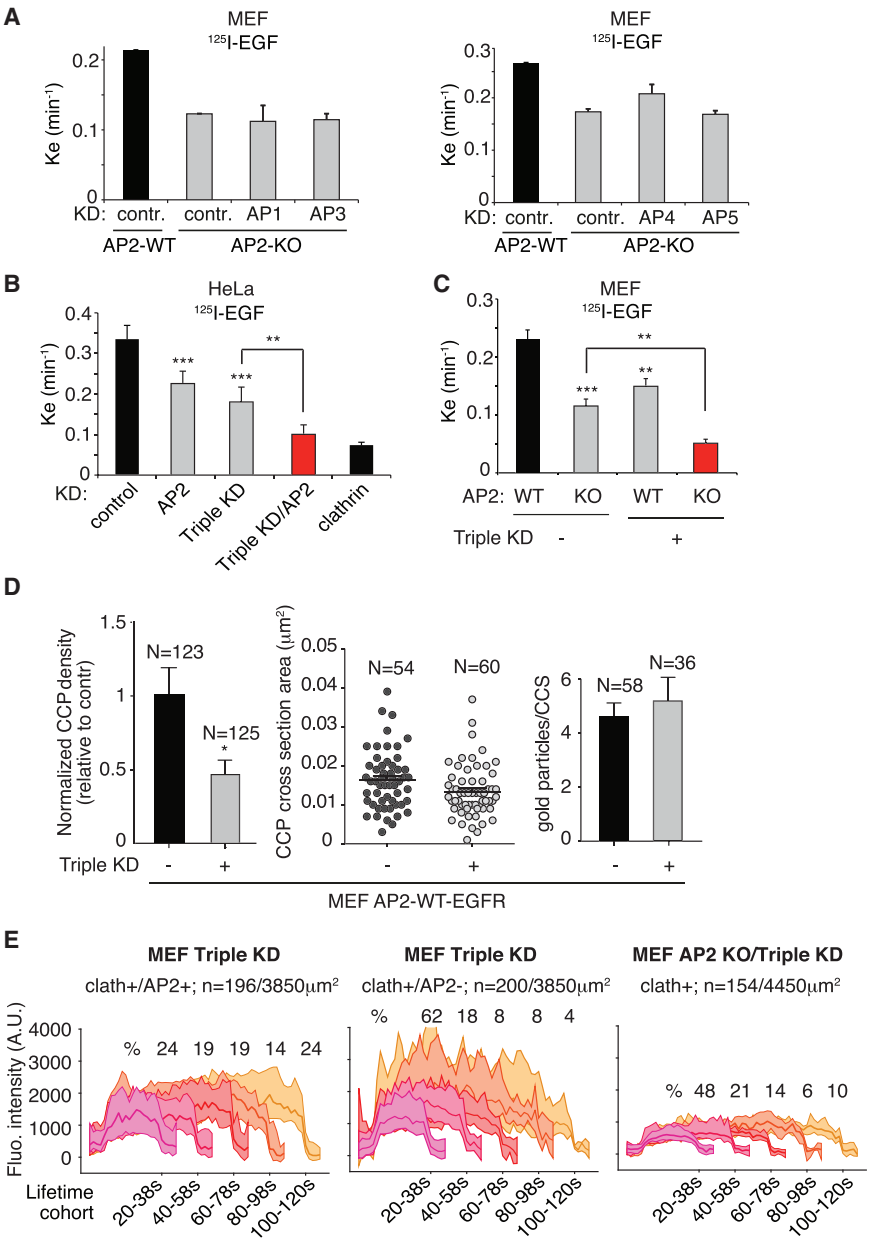

Figure 5. Mechanism of AP2-Independent EGFR-CME: Role of eps15/L1 and epsin1

(A) Transient KD of the μ subunit of the indicated AP complexes was performed in AP2-KO MEFs, and K_e of ^{125}I-EGF internalization was calculated. Data are mean ± SD (two replicates).

(B) K_e of ^{125}I-EGF internalization in stable eps15/eps15L1-KD HeLa cells transiently depleted of epsin1, alone or in combination with AP2μ, in comparison with AP2-KD and clathrin-KD HeLa cells. Results are mean ± SD of two to eight independent experiments. p values were calculated using each pair Student's t test (**p < 0.01 and ***p < 0.001).

(C) AP2-WT and AP2-KO MEFs were transiently depleted as indicated. K_e values of ^{125}I-EGF internalization are shown as mean ± SD of two independent experiments. p values were calculated using each pair Student's t test (**p < 0.01 and ***p < 0.001).

(D) TEM analysis of CCSs in AP2-WT-EGFR MEFs, control or triple KD for eps15, eps15L1, and epsin1, induced with doxycycline (to allow EGFR expression) and stimulated with EGF (30 ng/mL). Morphometrical analysis was performed on EGFR gold-positive structures. Left: CCP number was normalized for the difference in PM length between eps15/eps15L1/epsin1 KD MEFs versus control (~0.8 decrease; see Figure S3A and STAR Methods) and expressed relative to control cells. Right: mean number of gold particle per CCS (CCPs + CCVs). N represents the numbers of random images (left panel) and numbers of CCSs (center and right panels) analyzed. Data are expressed as mean ± SEM. p values were calculated using each pair Student's t test (*p < 0.05).

(E) Automated analysis of clathrin-coated structure formation at the plasma membrane from 196 traces containing CLTA-TagRFP and AP2σ-EGFP (clathrin+/AP2+; left panel), 200 traces devoid of AP2σ-EGFP (clathrin+/AP2−; middle panel) from 10 MEF AP2-WT/triple-KD, or 154 traces from 10 MEF AP2-KO/triple-KD cells (right panel).

to the PM (Figure 6A). The minimal interpretation of these data is that the function of AP2 is at least in part dispensable for the execution of one of the major tasks of endocytosis (i.e., long-term attenuation of signaling through receptor degradation). In fact, the opposite seems to be true, namely, AP2 might counteract this function, possibly by augmenting EGFR recycling to the PM, thereby helping modulate EGF-mediated signaling. This possibility was tested by analyzing signaling pathways triggered by the EGFR upon stimulation with low EGF doses in AP2-KO MEFs and AP2-KD HeLa cells. AP2-KO caused a significant attenuation of the phosphorylated AKT signal (Figures 6B and S6A), a readout for reduced PI3K activity (Vanhaesebroeck et al., 1997). The effect appeared to be rather specific for this signaling pathway, as the kinetics of phosphorylation of ERK1/2 and Shc were altered to a much lesser extent in the same cells (Figure 6B).

The attenuation in the magnitude of AKT phosphorylation was confirmed also in HeLa AP2-KD cells (Figures 6C and S6B). In contrast, triple-KD had only a minor impact, with a slight increase in the duration of the signal in both cell systems (Figures 6C, S6B, and S6C).

Given the established causal connection between the PI3K signaling pathway and growth factor-induced directed cell migration (Devreotes and Horwitz, 2015; Bear and Haugh, 2014), we tested the impact of AP2 on EGF-mediated chemotaxis. Importantly, AP2-KD in HeLa cells, but not triple-KD, caused a severe impairment in EGF-induced cell migration (Figure 6D). This defect was not observed when cells migrated in response to serum (Figure 6D), excluding a general impairment of the chemotactic response in AP2-KD cells and

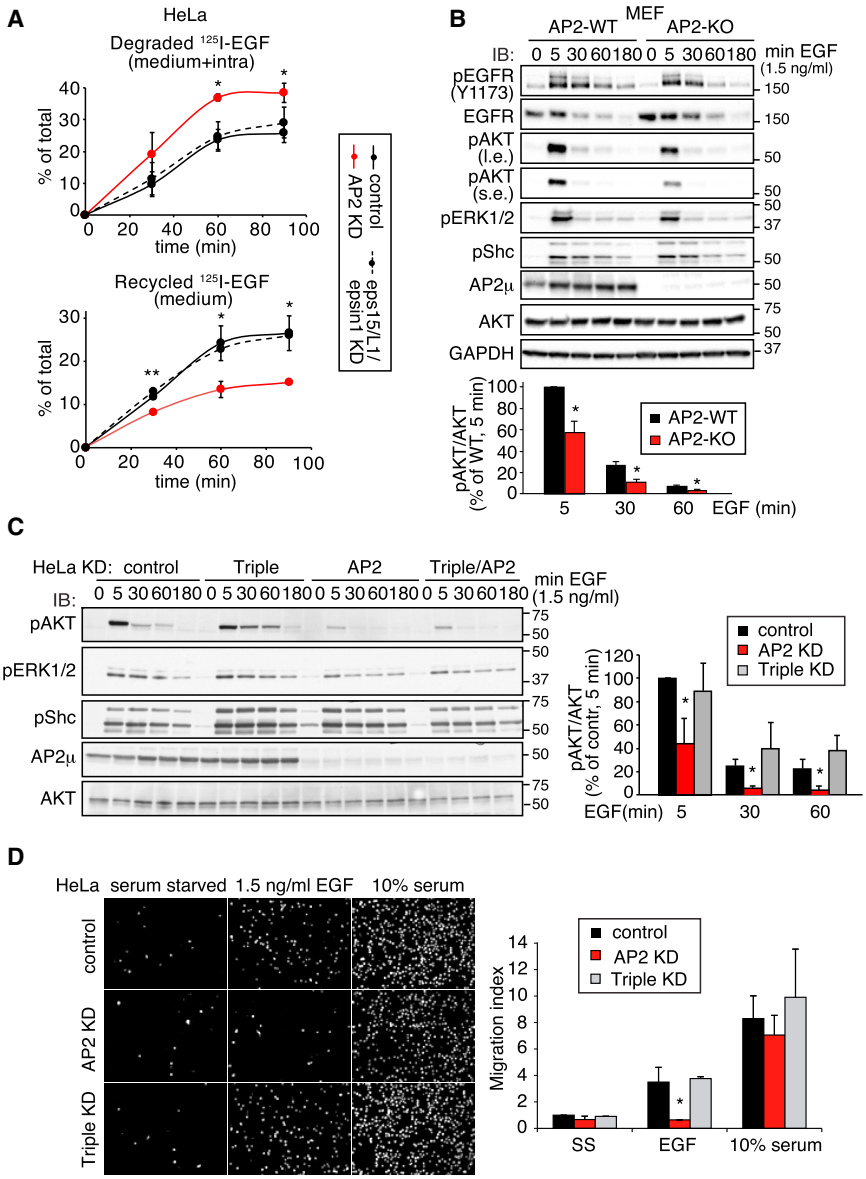

Figure 6. EGF-Dependent Signaling and Migration in AP2-Depleted Cells

(A) HeLa cells were subjected to AP2 KD or eps15/L1/epsin1 KD followed by ^{125}I-EGF degradation assay at low EGF concentration (1.5 ng/mL; see STAR Methods). At the indicated time points, (1) degraded EGF (top) represents the TCA soluble fraction of ^{125}I-EGF recovered in the medium and intracellularly, and (2) recycled EGF (bottom) represents the TCA insoluble fraction of ^{125}I-EGF recovered in the medium. Results are mean ± SD of two independent experiments. p values were calculated using each pair Student's t test (*p < 0.05 and **p < 0.01).

(B) Top: AP2-WT and AP2-KO MEFs were stimulated with low dose EGF (1.5 ng/mL) for the indicated times. Lysates were subjected to IB with the indicated antibodies. Bottom: quantitation of phosphoAKT signal normalized to total AKT (pAKT/AKT) and represented as percentage of signal in WT cells at 5 min of EGF stimulation. Results are mean ± SD of three independent experiments. p values were calculated using two-tailed Student's t test (*p < 0.05 versus WT at each time point).

(C) Left: HeLa cells were subjected to AP2 KD and/or eps15/L1/epsin1 KD in different combinations, followed by stimulation with low dose EGF (1.5 ng/mL) for the indicated times. IB was as shown. Right: quantitation of phosphoAKT signal normalized to total AKT (pAKT/AKT) and represented as percentage of signal in control cells at 5 min of EGF stimulation. Results are mean ± SD of three independent experiments. p values were calculated using two-tailed Student's t test. *p < 0.05 versus control at each time point.

(D) Transwell migration assay of AP2 KD and eps15/L1/epsin1 KD HeLa cells under serum-starved (SS) conditions or in the presence of low-dose EGF (1.5 ng/mL) or 10% serum as indicated. Right: quantitation of migrating cells per field. Results are the mean ± SD of two to four independent experiments. p values were calculated using two-tailed Student's t test (*p < 0.05 versus control in each condition).

arguing instead for a specific effect of AP2 on EGF-dependent migration.

Ultimately, EGFR activation results in the activation of transcriptional programs involving immediate-early genes (IEGs; at 30–45 min) (i.e., the transcription factors *FOS*, *EGR1*, *JUN*, and *JUNB*) and delayed early genes (DEGs; at 1–2 h), including *DUSP5* and *AREG* (Brankatschk et al., 2012; Avraham and Yarden, 2011; Avraham et al., 2010). The kinetics of these events are thought to define the specificity of the downstream transcriptional program (Golan-Lavi et al., 2017), determining the final cellular outcome.

In agreement with previous reports, IEGs were activated in HeLa cells stimulated with low EGF dose (or with serum), peaking at early time points (30–45 min) (Figure 7A, upper rows), while DEGs were activated at later times (1–2 h; Figure 7A, lower rows). No major differences were noticeable between the transcriptional profiles in HeLa and HeLa-AP2-KD cells (under EGF or serum stimulation) (Figure 7A). Some minor, statistically significant variations were detected, but the magnitude of the effects was minute and probably biologically inconsequential. These data argue that the migratory defect we observed in EGF-stimulated HeLa-AP2-KD cells is largely independent of the EGF-induced early transcriptional program and more likely dependent on the modification of protein activity that characterizes the cytoplasmic component of EGFR signaling.

The kinetics of EGF-induced transcriptional regulation were comparable between WT MEFs and HeLa cells. In contrast, AP2-KO led to sizable differences in gene expression of a subset of EGF-induced genes, such as (1) reduced induction (i.e., *FOS*), (2) delayed peak of activation (i.e., *JUN*, *DUSP5*, and *AREG*), and (3) increased and sustained activation (i.e., *AREG*) (Figure 7B). Thus, AP2 KO in MEFs appeared to have a selective effect on

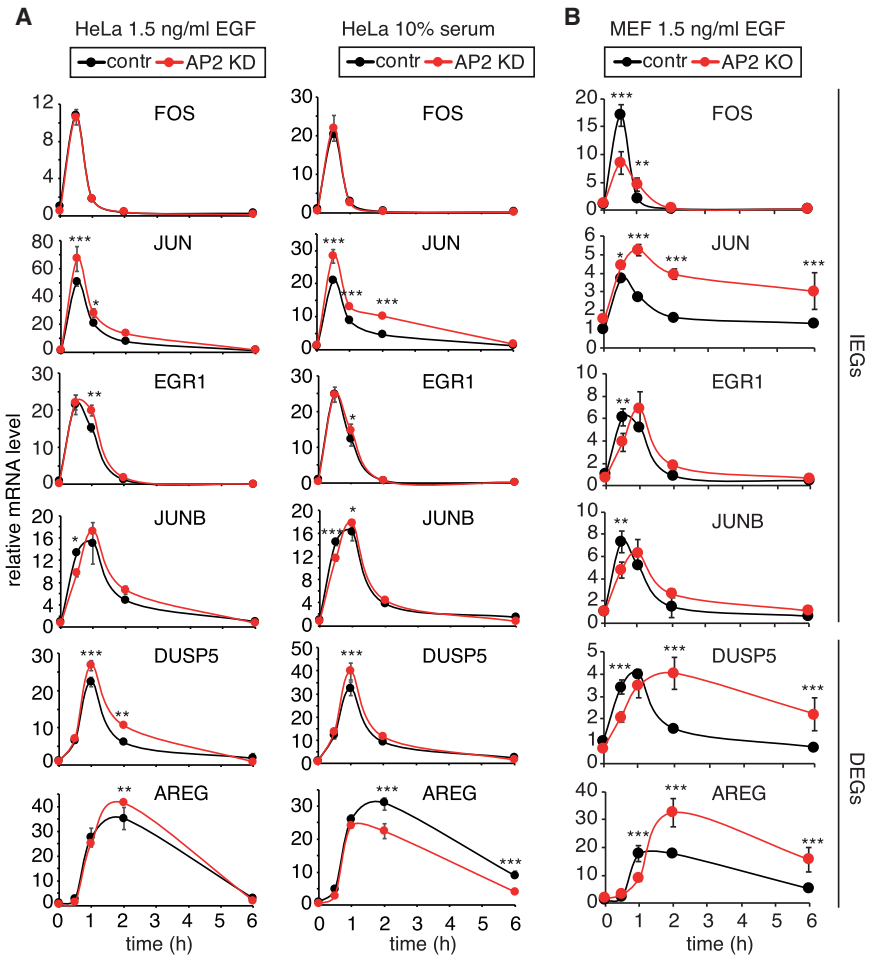

Figure 7. EGF-Dependent Transcriptional Output in AP2-Depleted Cells

(A) Control or AP2 KD HeLa cells were serum starved overnight followed by stimulation with low-dose EGF (1.5 ng/mL) or with complete medium (10% serum) for the indicated time points. Reported is the mRNA level, assessed by RT-qPCR, of the indicated genes, relative to the unstimulated control and normalized to the levels of the *RPLP0* housekeeping gene. Mean ± SD of two independent experiments with duplicates points is shown. (B) Control or AP2 KO MEFs were serum starved overnight, followed by stimulation with low-dose EGF (1.5 ng/mL) for the indicated time points. Data are expressed as in (A). Mean ± SD of three independent experiments with duplicate points is shown.

p values in (A) and (B) were calculated using each pair Student's t test (*$p < 0.05$, **$p < 0.01$, and ***$p < 0.001$).

the transcription of some EGF-induced genes. In addition, given the differences in the transcriptional impact of AP2 depletion in HeLa versus MEFs, some of the AP2-dependent effects on EGFR long-term signaling could be context specific.

DISCUSSION

We herein report the identification of distinct classes of CCPs that are molecularly distinguished by the presence or lack of AP2. Coupling the use of AP2-KO MEFs, combined with the KD of other adaptor proteins, we dissected the role of AP2-dependent and AP2-independent mechanisms in EGFR internalization and the consequences to the fate, signaling, and biological activities. Our data show that AP2, although not an absolute requirement for EGFR internalization and degradation, is crucial for the magnitude of certain EGFR-dependent signals and for at least one of its associated biological functions (i.e., cell migration).

Distinct Subclasses of CCPs

CCPs with different lifetimes and sizes have been detected in cells (Dambournet et al., 2018; Grove et al., 2014; Aguet et al., 2013; Cocucci et al., 2012; Henry et al., 2012; Doyon et al., 2011; Loerke et al., 2009; Puthenveedu and von Zastrow, 2006). We show that this reflects at least in part a specific molecular composition, defining the existence of at least two types of CCPs detected under physiological unperturbed conditions, characterized by the presence or absence of AP2 and by distinct dynamics and morphological features.

The dependency of the "different" types of pits on various endocytic proteins was explored by taking advantage of molecular genetics. In TIRF experiments, we exploited the genetically engineered deletion of AP2 (AP2-KO) and/or the simultaneous depletion of eps15/L1 and epsin1 adaptors (triple-KD). Our data suggest that (1) AP2 has a role in regulating CCP number, size and lifetime, as previously suggested (Dambournet et al., 2018; Kadlecova et al., 2017; Miller et al., 2015; Motley et al., 2003) and in agreement with recent findings that AP2 levels are finely regulated during cell differentiation with a consequent impact on CCP dynamics (Dambournet et al., 2018), and (2) one of the functions of eps15/L1 and epsin1 is to control, to a certain extent, the number of CCPs without affecting their dynamics.

One interesting observation that emerges from our study is that when all adaptor proteins (AP2-KO + triple-KD, henceforth KO/KD; Figure 5E, right) were removed, some CCPs persisted, although displaying significant reductions in number, size, and lifetime. This could be due to incomplete ablation of eps15/eps15L1/epsin1 or to participation of other endocytic proteins in CCP formation, as also supported by extant literature (Kaksonen and Roux, 2018; Mettlen et al., 2009; Merrifield et al., 2005). We favor the second possibility, because we showed that in the KO/KD cells, the internalization of the EGFR was reduced to background (clathrin-KD) levels, arguing for efficient ablation of the three adaptors.

AP2 and EGFR Internalization

At the functional level, we provided conclusive evidence, in a clean genetic background (i.e., KO of AP2), that the internalization of EGFR versus TfR depends differently on AP2, confirming previous observations (Johannessen et al., 2006; Maurer and Cooper, 2006; Huang et al., 2004; Hinrichsen et al., 2003; Motley et al., 2003). Although EGFR internalization was reduced but still functional in AP2-KO cells, TfR uptake was reduced to background levels.

One important question is how EGFR-CME proceeds in the absence of AP2. Our results point to a major role of eps15/L1 and epsin1 (by and large acting redundantly among themselves). We do not know whether (and if so how) the ''cargo adaptor'' function of these proteins is linked to that of regulating CCP number. However, in KO/KD cells (Figure 5E, right), small short-lived CCPs could still form, although they were incapable of supporting any significant internalization of EGF. Conversely, in the presence of eps15/L1 and epsin1 (AP2-KO), structures indistinguishable from those present in KO/KD cells were clearly sufficient to internalize a significant amount of EGF. Thus, the notion that eps15/L1 and epsin1 function as alternative adaptors to AP2 under physiological conditions is supported by experimental evidence and, at least in the case of epsin1, it was also previously suggested (Fortian et al., 2015; Bertelsen et al., 2011). However, our data do not imply a scenario of ''either AP2 or eps15/L1/epsin1,'' as they are equally compatible with eps15/L1 and epsin1 participating in all internalization events irrespective of the presence of AP2. Further experiments will be needed to address this issue.

Similarly, the molecular working of eps15/L1/epsin1 in AP2-independent CME remains to be resolved. Of note, these proteins are endowed with a dual biochemical property: (1) harboring ubiquitin-binding domains (UIMs), thereby binding to ubiquitinated proteins, and (2) being monoubiquitinated upon EGF treatment (Polo et al., 2002). One can postulate that through UIMs, they can be recruited to ubiquitinated EGFRs or that through monoubiquitination, they can generate protein-protein interactions, within the endocytic machinery, required for CME. The two functions are not mutually exclusive, and evidence both in favor (Fortian et al., 2015; Goh et al., 2010) and against (Sigismund et al., 2005, 2013) a critical role of EGFR ubiquitination in CME has been produced. Furthermore, we have previously shown that these adaptor proteins play a critical, redundant, role in CME, dependent on their ability to be ubiquitinated and deubiquitinated (Savio et al., 2016). The issue, therefore, remains open and will require further investigation.

AP2 and EGFR Fate, Signaling, and Biological Activity

When analyzing the fate of the internalized EGFR in the absence of AP2, we obtained a somewhat surprising result. AP2 appears to be dispensable (at least in part) for one of the major functions of endocytosis in the regulation of EGFR signaling (i.e., attenuation through degradation). This suggests the following interpretation. In the absence of AP2, EGFRs are internalized through eps15/L1/epsin1-dependent CCVs destined to degradation: a situation reminiscent of the ancestral mode based on ubiquitinated adaptors present in yeast (Lu et al., 2016). When AP2 is included, it possibly recruits other proteins responsible for committing the internalizing structures to recycling thereby diverting them from the degradative pathway. The molecular workings of the putative AP2-mediated recycling warrant further investigations.

At the signaling level, the impact of AP2, and presumably of CME, seems to be exerted at multiple levels. When analyzing the effects of AP2 ablation on the more proximal EGFR-dependent signaling, we detected decreased magnitude and duration of certain downstream signaling pathways, in agreement with previous reports showing that EGFR mutants with impaired AP2-binding sites display defects in AKT signaling (Goh et al., 2010). These effects were accompanied by attenuation of EGF-dependent cell migration. This latter effect did not involve perturbations of EGF-dependent transcriptional programs and is therefore likely due to alterations of the initial chain of EGFR-dependent transduction events. In this contention, we note that clustering of signaling receptors into CCPs has been proposed as a mechanism to regulate signaling magnitude at the PM (reviewed by Barbieri et al., 2016). In particular, EGFR recruitment into CCPs was proposed to spatially constrain otherwise short-lived EGFR dimers and to amplify receptor activation (Rosselli-Murai et al., 2018; Ibach et al., 2015). Thus, AP2 might be instrumental in assembling PM-based signaling platforms. This possibility is not mutually exclusive with that of prolonged signaling from an early endosomal compartment, which would be sustained through repeated AP2-dependent cycles of internalization and recycling.

Finally, when we analyzed the effects of AP2 depletion on the EGFR-induced transcriptional effects, a clear context dependency emerged. Although we cannot formally rule out that the effects were due to different extents of AP2 ablation, in HeLa AP2-KD versus MEF AP2-KO, we note that all the evidence presented in this study indicates that under our conditions, the KD and the KO phenocopy each other. Thus, we favor the interpretation that there is cell-specific variability in the impact of CME in determining the final EGFR signaling outcome. This is in line with recent findings showing that AP2 levels are variable in different isogenic cellular contexts (Dambournet et al., 2018), unveiling an unexpected level of plasticity of CME underlying the different specifications required in various cell types.

STAR★METHODS

Detailed methods are provided in the online version of this paper and include the following:

- KEY RESOURCES TABLE
- CONTACT FOR REAGENT AND RESOURSE SHARING
- EXPERIMENTAL MODEL AND SUBJECT DETAILS
- METHOD DETAILS
  - EGF **concentrations, constructs and antibodies**
  - CRE treatment of AP2$\mu^{fl/fl}$ MEFs
  - Genome editing of SUM159 cells using the TALEN-based approach
  - TIRF based live-cell microscopy imaging and analysis
  - RNAi experiments
  - Quantitative real-time PCR analysis
  - Cell lysis and immunoblot (IB)

- Radioactive assays
- Cell migration assay
- Plasma membrane sheets (PMS)
- Transmission Electron Microscopy (TEM)
- Pre-embedding immunolabeling
- Anti-EGF immunolabeling of cryosections
- Analysis of cell surface area and perimeter

● QUANTIFICATION AND STATISTICAL ANALYSIS

SUPPLEMENTAL INFORMATION

Supplemental Information can be found online at https://doi.org/10.1016/j.celrep.2019.05.017.

ACKNOWLEDGMENTS

We thank Rosalind Gunby for critically reading the manuscript. We are grateful to the ALEMBIC facility at San Raffaele Scientific Institute (Milan, Italy) for support in EM analysis. We thank E. Villa, IEO Milan, for a script in the CME package that facilitates CCP tracing. This work was supported by grants from Worldwide Cancer Research (16-1245) to S.S.; Associazione Italiana per la Ricerca sul Cancro to P.P.D.F. (AIRC IG 18988 and MCO 10.000) and to S.P. (AIRC IG 15637); the Italian Ministry of University and Scientific Research (MIUR) to C. Tacchetti and P.P.D.F. (PRIN 2015XS92CC); and the Italian Ministry of Health to P.P.D.F. V.H. and T.M. acknowledge support from Deutsche Forschungsgemeinschaft (DFG; SFB958/A01 to V.H. and T.M. and HA2686/13-1 to V.H.). A.C. is supported by a fellowship from Fondazione Umberto Veronesi. E.B. was supported by a FIRC-AIRC fellowship. T.K., M.P., and S.U. were funded by grants from Biogen and Ionis Pharmaceuticals and by NIH grants R01GM075252 and 5U19AI109740-05 (to T.K.). S.U. is a fellow at the Image and Data Analysis core at Harvard Medical School.

AUTHOR CONTRIBUTIONS

R.P. and V.A. performed most of the experiments in AP2 MEFs and HeLa cells. A.C. performed the signaling experiments. A.R. conducted the EM experiments. M.P. and S.U. performed the live imaging analysis. R.G. generated the SUM159 gene-edited cells. T.M. generated the AP2$\mu^{fl/fl}$ mice; E.B. and G.C. prepared samples for EM analysis. C. Tordonato performed the transcriptomic analysis. S.C. performed the statistical analysis. S.F. performed the cell surface analysis. M.G.M. contributed to paper writing. E.M. and S.P. generated the double eps15/eps15L1 HeLa cells and contributed to result interpretation. C. Tacchetti coordinated the EM experiments. V.H. generated the AP2$\mu^{fl/fl}$ mice and contributed to result interpretation. T.K. and P.P.D.F. contributed to the experimental design and writing the paper. S.S. coordinated the team, designed the experiments, and wrote the paper.

DECLARATION OF INTERESTS

The authors declare no competing interests.

Received: December 17, 2018
Revised: April 4, 2019
Accepted: May 2, 2019
Published: June 4, 2019

REFERENCES

Aguet, F., Antonescu, C.N., Mettlen, M., Schmid, S.L., and Danuser, G. (2013). Advances in analysis of low signal-to-noise images link dynamin and AP2 to the functions of an endocytic checkpoint. Dev. Cell *26*, 279–291.

Aguet, F., Upadhyayula, S., Gaudin, R., Chou, Y.Y., Cocucci, E., He, K., Chen, B.C., Mosaliganti, K., Pasham, M., Skillern, W., et al. (2016). Membrane dynamics of dividing cells imaged by lattice light-sheet microscopy. Mol. Biol. Cell *27*, 3418–3435.

Antonny, B., Burd, C., De Camilli, P., Chen, E., Daumke, O., Faelber, K., Ford, M., Frolov, V.A., Frost, A., Hinshaw, J.E., et al. (2016). Membrane fission by dynamin: what we know and what we need to know. EMBO J. *35*, 2270–2284.

Avraham, R., and Yarden, Y. (2011). Feedback regulation of EGFR signalling: decision making by early and delayed loops. Nat. Rev. Mol. Cell Biol. *12*, 104–117.

Avraham, R., Sas-Chen, A., Manor, O., Steinfeld, I., Shalgi, R., Tarcic, G., Bossel, N., Zeisel, A., Amit, I., Zwang, Y., et al. (2010). EGF decreases the abundance of microRNAs that restrain oncogenic transcription factors. Sci. Signal. *3*, ra43.

Barbieri, E., Di Fiore, P.P., and Sigismund, S. (2016). Endocytic control of signaling at the plasma membrane. Curr. Opin. Cell Biol. *39*, 21–27.

Bear, J.E., and Haugh, J.M. (2014). Directed migration of mesenchymal cells: where signaling and the cytoskeleton meet. Curr. Opin. Cell Biol. *30*, 74–82.

Bertelsen, V., Sak, M.M., Breen, K., Rødland, M.S., Johannessen, L.E., Traub, L.M., Stang, E., and Madshus, I.H. (2011). A chimeric pre-ubiquitinated EGF receptor is constitutively endocytosed in a clathrin-dependent, but kinase-independent manner. Traffic *12*, 507–520.

Boucrot, E., Saffarian, S., Zhang, R., and Kirchhausen, T. (2010). Roles of AP-2 in clathrin-mediated endocytosis. PLoS One *5*, e10597.

Brach, T., Godlee, C., Moeller-Hansen, I., Boeke, D., and Kaksonen, M. (2014). The initiation of clathrin-mediated endocytosis is mechanistically highly flexible. Curr. Biol. *24*, 548–554.

Brankatschk, B., Wichert, S.P., Johnson, S.D., Schaad, O., Rossner, M.J., and Gruenberg, J. (2012). Regulation of the EGF transcriptional response by endocytic sorting. Sci. Signal. *5*, ra21.

Caldieri, G., Barbieri, E., Nappo, G., Raimondi, A., Bonora, M., Conte, A., Verhoef, L.G.G.C., Confalonieri, S., Malabarba, M.G., Bianchi, F., et al. (2017). Reticulon 3-dependent ER-PM contact sites control EGFR nonclathrin endocytosis. Science *356*, 617–624.

Carroll, S.Y., Stimpson, H.E., Weinberg, J., Toret, C.P., Sun, Y., and Drubin, D.G. (2012). Analysis of yeast endocytic site formation and maturation through a regulatory transition point. Mol. Biol. Cell *23*, 657–668.

Cocucci, E., Aguet, F., Boulant, S., and Kirchhausen, T. (2012). The first five seconds in the life of a clathrin-coated pit. Cell *150*, 495–507.

Cocucci, E., Gaudin, R., and Kirchhausen, T. (2014). Dynamin recruitment and membrane scission at the neck of a clathrin-coated pit. Mol. Biol. Cell *25*, 3595–3609.

Conte, A., and Sigismund, S. (2017). Methods to investigate EGFR ubiquitination. Methods Mol. Biol. *1652*, 81–100.

Dambournet, D., Sochacki, K.A., Cheng, A.T., Akamatsu, M., Taraska, J.W., Hockemeyer, D., and Drubin, D.G. (2018). Genome-edited human stem cells expressing fluorescently labeled endocytic markers allow quantitative analysis of clathrin-mediated endocytosis during differentiation. J. Cell Biol. *217*, 3301–3311.

Devreotes, P., and Horwitz, A.R. (2015). Signaling networks that regulate cell migration. Cold Spring Harb. Perspect. Biol. *7*, a005959.

Doyon, J.B., Zeitler, B., Cheng, J., Cheng, A.T., Cherone, J.M., Santiago, Y., Lee, A.H., Vo, T.D., Doyon, Y., Miller, J.C., et al. (2011). Rapid and efficient clathrin-mediated endocytosis revealed in genome-edited mammalian cells. Nat. Cell Biol. *13*, 331–337.

Ehrlich, M., Boll, W., Van Oijen, A., Hariharan, R., Chandran, K., Nibert, M.L., and Kirchhausen, T. (2004). Endocytosis by random initiation and stabilization of clathrin-coated pits. Cell *118*, 591–605.

Fortian, A., Dionne, L.K., Hong, S.H., Kim, W., Gygi, S.P., Watkins, S.C., and Sorkin, A. (2015). Endocytosis of ubiquitylation-deficient EGFR mutants via clathrin-coated pits is mediated by ubiquitylation. Traffic *16*, 1137–1154.

Goh, L.K., Huang, F., Kim, W., Gygi, S., and Sorkin, A. (2010). Multiple mechanisms collectively regulate clathrin-mediated endocytosis of the epidermal growth factor receptor. J. Cell Biol. *189*, 871–883.

Golan-Lavi, R., Giacomelli, C., Fuks, G., Zeisel, A., Sonntag, J., Sinha, S., Köstler, W., Wiemann, S., Korf, U., Yarden, Y., and Domany, E. (2017).

Coordinated pulses of mRNA and of protein translation or degradation produce EGF-induced protein bursts. Cell Rep. *18*, 3129–3142.

González-Gaitán, M., and Jäckle, H. (1997). Role of Drosophila alpha-adaptin in presynaptic vesicle recycling. Cell *88*, 767–776.

Grove, J., Metcalf, D.J., Knight, A.E., Wavre-Shapton, S.T., Sun, T., Protonotarios, E.D., Griffin, L.D., Lippincott-Schwartz, J., and Marsh, M. (2014). Flat clathrin lattices: stable features of the plasma membrane. Mol. Biol. Cell *25*, 3581–3594.

Gu, M., Schuske, K., Watanabe, S., Liu, Q., Baum, P., Garriga, G., and Jorgensen, E.M. (2008). Mu2 adaptin facilitates but is not essential for synaptic vesicle recycling in Caenorhabditis elegans. J. Cell Biol. *183*, 881–892.

He, K., Marsland, R., III, Upadhyayula, S., Song, E., Dang, S., Capraro, B.R., Wang, W., Skillern, W., Gaudin, R., Ma, M., and Kirchhausen, T. (2017). Dynamics of phosphoinositide conversion in clathrin-mediated endocytic traffic. Nature *552*, 410–414.

Henry, A.G., Hislop, J.N., Grove, J., Thorn, K., Marsh, M., and von Zastrow, M. (2012). Regulation of endocytic clathrin dynamics by cargo ubiquitination. Dev. Cell *23*, 519–532.

Hinrichsen, L., Harborth, J., Andrees, L., Weber, K., and Ungewickell, E.J. (2003). Effect of clathrin heavy chain- and alpha-adaptin-specific small inhibitory RNAs on endocytic accessory proteins and receptor trafficking in HeLa cells. J. Biol. Chem. *278*, 45160–45170.

Huang, F., Khvorova, A., Marshall, W., and Sorkin, A. (2004). Analysis of clathrin-mediated endocytosis of epidermal growth factor receptor by RNA interference. J. Biol. Chem. *279*, 16657–16661.

Ibach, J., Radon, Y., Gelléri, M., Sonntag, M.H., Brunsveld, L., Bastiaens, P.I., and Verveer, P.J. (2015). Single particle tracking reveals that EGFR signaling activity is amplified in clathrin-coated pits. PLoS One *10*, e0143162.

Johannessen, L.E., Pedersen, N.M., Pedersen, K.W., Madshus, I.H., and Stang, E. (2006). Activation of the epidermal growth factor (EGF) receptor induces formation of EGF receptor- and Grb2-containing clathrin-coated pits. Mol. Cell. Biol. *26*, 389–401.

Kadlecova, Z., Spielman, S.J., Loerke, D., Mohanakrishnan, A., Reed, D.K., and Schmid, S.L. (2017). Regulation of clathrin-mediated endocytosis by hierarchical allosteric activation of AP2. J. Cell Biol. *216*, 167–179.

Kaksonen, M., and Roux, A. (2018). Mechanisms of clathrin-mediated endocytosis. Nat. Rev. Mol. Cell Biol. *19*, 313–326.

Kelly, B.T., Graham, S.C., Liska, N., Dannhauser, P.N., Höning, S., Ungewickell, E.J., and Owen, D.J. (2014). Clathrin adaptors. AP2 controls clathrin polymerization with a membrane-activated switch. Science *345*, 459–463.

Kirchhausen, T. (1990). Identification of a putative yeast homolog of the mammalian beta chains of the clathrin-associated protein complexes. Mol. Cell. Biol. *10*, 6089–6090.

Kirchhausen, T., Owen, D., and Harrison, S.C. (2014). Molecular structure, function, and dynamics of clathrin-mediated membrane traffic. Cold Spring Harb. Perspect. Biol. *6*, a016725.

Kononenko, N.L., Puchkov, D., Classen, G.A., Walter, A.M., Pechstein, A., Sawade, L., Kaempf, N., Trimbuch, T., Lorenz, D., Rosenmund, C., et al. (2014). Clathrin/AP-2 mediate synaptic vesicle reformation from endosome-like vacuoles but are not essential for membrane retrieval at central synapses. Neuron *82*, 981–988.

Liu, A.P., Aguet, F., Danuser, G., and Schmid, S.L. (2010). Local clustering of transferrin receptors promotes clathrin-coated pit initiation. J. Cell Biol. *191*, 1381–1393.

Loerke, D., Mettlen, M., Yarar, D., Jaqaman, K., Jaqaman, H., Danuser, G., and Schmid, S.L. (2009). Cargo and dynamin regulate clathrin-coated pit maturation. PLoS Biol. *7*, e57.

Lu, R., Drubin, D.G., and Sun, Y. (2016). Clathrin-mediated endocytosis in budding yeast at a glance. J. Cell Sci. *129*, 1531–1536.

Maurer, M.E., and Cooper, J.A. (2006). The adaptor protein Dab2 sorts LDL receptors into coated pits independently of AP-2 and ARH. J. Cell Sci. *119*, 4235–4246.

McMahon, H.T., and Boucrot, E. (2011). Molecular mechanism and physiological functions of clathrin-mediated endocytosis. Nat. Rev. Mol. Cell Biol. *12*, 517–533.

Merrifield, C.J., and Kaksonen, M. (2014). Endocytic accessory factors and regulation of clathrin-mediated endocytosis. Cold Spring Harb. Perspect. Biol. *6*, a016733.

Merrifield, C.J., Perrais, D., and Zenisek, D. (2005). Coupling between clathrin-coated-pit invagination, cortactin recruitment, and membrane scission observed in live cells. Cell *121*, 593–606.

Mettlen, M., Stoeber, M., Loerke, D., Antonescu, C.N., Danuser, G., and Schmid, S.L. (2009). Endocytic accessory proteins are functionally distinguished by their differential effects on the maturation of clathrin-coated pits. Mol. Biol. Cell *20*, 3251–3260.

Miller, S.E., Mathiasen, S., Bright, N.A., Pierre, F., Kelly, B.T., Kladt, N., Schauss, A., Merrifield, C.J., Stamou, D., Höning, S., and Owen, D.J. (2015). CALM regulates clathrin-coated vesicle size and maturation by directly sensing and driving membrane curvature. Dev. Cell *33*, 163–175.

Mitsunari, T., Nakatsu, F., Shioda, N., Love, P.E., Grinberg, A., Bonifacino, J.S., and Ohno, H. (2005). Clathrin adaptor AP-2 is essential for early embryonal development. Mol. Cell. Biol. *25*, 9318–9323.

Motley, A., Bright, N.A., Seaman, M.N., and Robinson, M.S. (2003). Clathrin-mediated endocytosis in AP-2-depleted cells. J. Cell Biol. *162*, 909–918.

Nakayama, Y., Goebl, M., O'Brine Greco, B., Lemmon, S., Pingchang Chow, E., and Kirchhausen, T. (1991). The medium chains of the mammalian clathrin-associated proteins have a homolog in yeast. Eur. J. Biochem. *202*, 569–574.

Penengo, L., Mapelli, M., Murachelli, A.G., Confalonieri, S., Magri, L., Musacchio, A., Di Fiore, P.P., Polo, S., and Schneider, T.R. (2006). Crystal structure of the ubiquitin binding domains of rabex-5 reveals two modes of interaction with ubiquitin. Cell *124*, 1183–1195.

Pinilla-Macua, I., and Sorkin, A. (2015). Methods to study endocytic trafficking of the EGF receptor. Methods Cell Biol. *130*, 347–367.

Polo, S., Sigismund, S., Faretta, M., Guidi, M., Capua, M.R., Bossi, G., Chen, H., De Camilli, P., and Di Fiore, P.P. (2002). A single motif responsible for ubiquitin recognition and monoubiquitination in endocytic proteins. Nature *416*, 451–455.

Pozzi, B., Amodio, S., Lucano, C., Sciullo, A., Ronzoni, S., Castelletti, D., Adler, T., Treise, I., Betsholtz, I.H., Rathkolb, B., et al. (2012). The endocytic adaptor Eps15 controls marginal zone B cell numbers. PLoS One *7*, e50818.

Puthenveedu, M.A., and von Zastrow, M. (2006). Cargo regulates clathrin-coated pit dynamics. Cell *127*, 113–124.

Robinson, M.S. (2015). Forty years of clathrin-coated vesicles. Traffic *16*, 1210–1238.

Rosselli-Murai, L.K., Yates, J.A., Yoshida, S., Bourg, J., Ho, K.K.Y., White, M., Prisby, J., Tan, X., Altemus, M., Bao, L., et al. (2018). Loss of PTEN promotes formation of signaling-capable clathrin-coated pits. J. Cell Sci. *131*, jcs208926.

Saffarian, S., Cocucci, E., and Kirchhausen, T. (2009). Distinct dynamics of endocytic clathrin-coated pits and coated plaques. PLoS Biol. *7*, e1000191.

Sanan, D.A., and Anderson, R.G. (1991). Simultaneous visualization of LDL receptor distribution and clathrin lattices on membranes torn from the upper surface of cultured cells. J. Histochem. Cytochem. *39*, 1017–1024.

Sanjana, N.E., Cong, L., Zhou, Y., Cunniff, M.M., Feng, G., and Zhang, F. (2012). A transcription activator-like effector toolbox for genome engineering. Nat. Protoc. *7*, 171–192.

Savio, M.G., Wollscheid, N., Cavallaro, E., Algisi, V., Di Fiore, P.P., Sigismund, S., Maspero, E., and Polo, S. (2016). USP9X controls EGFR fate by deubiquitinating the endocytic adaptor Eps15. Curr. Biol. *26*, 173–183.

Schledzewski, K., Brinkmann, H., and Mendel, R.R. (1999). Phylogenetic analysis of components of the eukaryotic vesicle transport system reveals a common origin of adaptor protein complexes 1, 2, and 3 and the F subcomplex of the coatomer COPI. J. Mol. Evol. *48*, 770–778.

Shin, K.J., Wall, E.A., Zavzavadjian, J.R., Santat, L.A., Liu, J., Hwang, J.I., Rebres, R., Roach, T., Seaman, W., Simon, M.I., and Fraser, I.D. (2006). A single lentiviral vector platform for microRNA-based conditional RNA interference and coordinated transgene expression. Proc. Natl. Acad. Sci. USA *103*, 13759–13764.

Sigismund, S., Woelk, T., Puri, C., Maspero, E., Tacchetti, C., Transidico, P., Di Fiore, P.P., and Polo, S. (2005). Clathrin-independent endocytosis of ubiquitinated cargos. Proc. Natl. Acad. Sci. USA *102*, 2760–2765.

Sigismund, S., Argenzio, E., Tosoni, D., Cavallaro, E., Polo, S., and Di Fiore, P.P. (2008). Clathrin-mediated internalization is essential for sustained EGFR signaling but dispensable for degradation. Dev. Cell *15*, 209–219.

Sigismund, S., Algisi, V., Nappo, G., Conte, A., Pascolutti, R., Cuomo, A., Bonaldi, T., Argenzio, E., Verhoef, L.G., Maspero, E., et al. (2013). Threshold-controlled ubiquitination of the EGFR directs receptor fate. EMBO J. *32*, 2140–2157.

Slot, J.W., and Geuze, H.J. (2007). Cryosectioning and immunolabeling. Nat. Protoc. *2*, 2480–2491.

Sorkin, A., Waters, C., Overholser, K.A., and Carpenter, G. (1991). Multiple autophosphorylation site mutations of the epidermal growth factor receptor. Analysis of kinase activity and endocytosis. J. Biol. Chem. *266*, 8355–8362.

Soykan, T., Maritzen, T., and Haucke, V. (2016). Modes and mechanisms of synaptic vesicle recycling. Curr. Opin. Neurobiol. *39*, 17–23.

Uphoff, C.C., and Drexler, H.G. (2002). Comparative PCR analysis for detection of mycoplasma infections in continuous cell lines. In Vitro Cell. Dev. Biol. Anim. *38*, 79–85.

Vanhaesebroeck, B., Leevers, S.J., Panayotou, G., and Waterfield, M.D. (1997). Phosphoinositide 3-kinases: a conserved family of signal transducers. Trends Biochem. Sci. *22*, 267–272.

Weinberg, J., and Drubin, D.G. (2012). Clathrin-mediated endocytosis in budding yeast. Trends Cell Biol. *22*, 1–13.

Weinberg, J.S., and Drubin, D.G. (2014). Regulation of clathrin-mediated endocytosis by dynamic ubiquitination and deubiquitination. Curr. Biol. *24*, 951–959.

STAR★METHODS

KEY RESOURCES TABLE

REAGENT or RESOURCE	SOURCE	IDENTIFIER
Antibodies		
Rabbit polyclonal anti-EGFR (epitope: aa 1172-1186, *Homo sapiens*)	In house	N/A
Mouse anti-eps15 (epitope: aa 2-330, *Mus musculus*)	In house	N/A
Rabbit anti-eps15L1 (epitope: aa 216-266, *Mus musculus*)	In house	N/A
Mouse anti-epsin1/2 (epitope: aa 249-401 of epsin1, *Homo sapiens*)	In house	N/A
Mouse anti-EGFR 13A9	Genentech	mAbEGFR 13A9
Anti-Alexa Fluor 488	ThermoFisher	Cat# A-11094, RRID:AB_221544
Anti-clathrin heavy chain (clone 23)	Transduction BD	Cat#610499, RRID:AB_397865
anti-AP2μ	Transduction BD	Cat#611350, RRID:AB_398872
Anti-AP2α	Sigma-Aldrich	Cat#A4325, RRID:AB_258156
Anti-AP2β	Sigma-Aldrich	Cat#A4325, RRID:AB_258156
Anti-AP2σ	Abcam	Cat#ab128950, RRID:AB_11140842
Anti-Phosphotyrosine Antibody, clone 4G10	Millipore-Merck	Cat#05-321 RRID:AB_309678
Anti-pShc	Cell Signaling	Cat#2434, RRID:AB_10841301
Anti-phospho-AKT (Ser473)	Cell Signaling	Cat#9271 RRID:AB_329825
Anti-phospho-ERK1/2 (Thr202/Tyr204)	Cell Signaling	Cat#9101, RRID:AB_331646
Anti-total-AKT	Cell Signaling	Cat#9272, RRID:AB_329827
Anti-total-ERK1/2	Sigma-Aldrich	Cat# M7927, RRID:AB_260665
Anti-pEGFR (Y1173)	Cell Signaling	Cat# 4407, RRID:AB_331795
Anti-GAPDH	Santa Cruz Biotechnology	Cat# sc-32233, RRID:AB_627679
Anti-tubulin	Millipore	Cat# MAB1864, RRID:AB_2210391
Anti-vinculin	Sigma-Aldrich	Cat# V9131, RRID:AB_477629
Chemicals, Peptides, and Recombinant Proteins		
Recombinant human EGF	BPSBioscience	Cat#90201-3
^{125}I-EGF	PerkinElmer	Cat#NEX428
^{125}I-Tf	PerkinElmer	Cat#NEX212
Alexa488-EGF	Molecular Probes	Cat#E13345
Recombinant TAT-Cre recombinase	In house	N/A
Protein-A Gold 10 nm	Utrecht University	Cat#PAG10nm
EM grade glutaraldehyde	Electron Microscopy Sciences	Cat#16210
Sodium cacodylate trihydrate	Sigma	Cat#C4945
Osmium tetroxide 4% SOL.10X10ML	Electron Microscopy Sciences	Cat#19190
Potassium ferricyanide	Electron Microscopy Sciences	Cat# 20150
Ruthenium red	Sigma	Cat#84071
Absolute ethanol	Sigma	Cat#32221-M
Epoxy embedding medium	Sigma	Cat#45359-1EA-F
Secondary rabbit anti-mouse IgG	Sigma	Cat# M7023, RRID:AB_260634
Collagen I rat tail	BD Bioscience	Cat#354236

(*Continued on next page*)

Continued

REAGENT or RESOURCE	SOURCE	IDENTIFIER
Critical Commercial Assays		
RNeasy kit	QIAGEN	Cat#74106
QuantiTect Reverse Transcription Kit	QIAGEN	Cat#205313
Inventoried Taqman assay, EPN1	Applied Biosystems	Hs00203391_m1
Inventoried Taqman assay, EPN2	Applied Biosystems	Hs00209150_m1
Inventoried Taqman assay, EPN3	Applied Biosystems	Hs00978957_m1
Inventoried Taqman assay, Epn1	Applied Biosystems	Mm01328492_m1
Inventoried Taqman assay, Epn2	Applied Biosystems	Mm00665982_g1
Inventoried Taqman assay, Epn3	Applied Biosystems	Mm00660955_m1
Inventoried Taqman assay, Cltc	Applied Biosystems	Mm01303974_m1
Inventoried Taqman assay, Ap1m1	Applied Biosystems	Mm00475912_m1
Inventoried Taqman assay, Ap1m2	Applied Biosystems	Mm00477565_m1
Inventoried Taqman assay, Ap2m1	Applied Biosystems	Mm01702796_g1
Inventoried Taqman assay, Ap3m1	Applied Biosystems	Mm00785907_s1
Inventoried Taqman assay, Ap3m2	Applied Biosystems	Mm00512819_m1
Inventoried Taqman assay, Ap4m1	Applied Biosystems	Mm00480494_m1
Inventoried Taqman assay, Ap5m1	Applied Biosystems	Mm00513794_m1
Inventoried Taqman assay, Gapdh	Applied Biosystems	mm99999915_g1
Inventoried Taqman assay, 18S	Applied Biosystems	Hs99999901_s1
miRneasy kit	QIAGEN	Cat#217004
SuperScript VILO cDNA Synthesis Kit	Invitrogen	Cat#11754050
hsa-Stat3	Quantitect	QT00068754
Experimental Models: Cell Lines		
HeLa cells	In house (Sigismund et al., 2013)	N/A
SUM159 cells gene edited to express AP2σ2-EGFP and CLTA-TagRFP	This paper	N/A
$AP2\mu^{fl/fl}$ MEFs	This paper	N/A
Oligonucleotides		
All Stars control siRNA	QIAGEN	Cat #1027280
Stealth RNAi, Clathrin Heavy Chain GAAGAACUCUUUG CCCGGAAAUUUA	ThermoFisher	N/A
RNAi, AP2α human AAGAGCAUGUGCACGCUGGCCA	Dharmacon (Motley et al., 2003)	N/A
iBONI siRNA, AP2μ human UGACCCGAAAGGCAUCCACCCCC	Riboxx	N/A
Stealth RNAi, epsin1 human UUACAAGGCCAUGACGCUGAUGGAG	ThermoFisher	N/A
Stealth RNAi, epsin1 mouse GACUGGCUCUGAGGCUGUAUCACAA	ThermoFisher	N/A
iBONI siRNA, eps15 mouse AAUACUCUCCCUUUGAACUUCCCCC	Riboxx	N/A
iBONI siRNA, eps15L1 mouse UUUCAAAGAUGCCAUCAAACCCCC	Riboxx	N/A
Stealth RNAi, epsin 2 human AAGAAAGCCGAAGGGACACAGUUAA	ThermoFisher	N/A
iBONI siRNA, AP1μ mouse UUCUUCCGAUACUUGAUGCCCCC	Riboxx	N/A
iBONI siRNA, AP3μ1 mouse UAAAUGGCUUAUACUUCUCCCCC	Riboxx	N/A
iBONI siRNA, AP3μ2 mouse UACAUCCCAAGACAGCAUCCCCC	Riboxx	N/A
iBONI siRNA, AP4μ mouse, pool of four oligos	Riboxx	N/A
iBONI siRNA, AP5μ mouse AUAAUCCAGACCAGUAAGCCCCC	Riboxx	N/A
Custom RT-qPCR primers for EGF-induced transcriptomic analysis	See Table S1	See Table S1
Recombinant DNA		
pMSCV- CLTA-TagRFP	Cocucci et al., 2012	N/A
pMSCV-AP2σ2-EGFP	Cocucci et al., 2012	N/A

(*Continued on next page*)

Continued

REAGENT or RESOURCE	SOURCE	IDENTIFIER
pSLIK-EGFR	This paper	N/A
pSLIK-neo lentiviral vector	Addgene (Shin et al., 2006)	Cat#25735
pSICOR-shRNA human eps15	Sigismund et al., 2005	N/A
pSICOR-shRNA human eps15L1	Sigismund et al., 2005	N/A
Software and Algorithms		
cmeAnalysis software package	Aguet et al., 2013	N/A

CONTACT FOR REAGENT AND RESOURSE SHARING

Further information and requests for resources and reagents should be directed to and will be fulfilled by the Lead Contact, Sara Sigismund (sara.sigismund@ieo.it).

EXPERIMENTAL MODEL AND SUBJECT DETAILS

HeLa cells (cervical cancer, female) were cultured were grown at 37°C and 5% CO_2 in GlutaMAX-Minimum Essential Medium (MEM, GIBCO Invitrogen), supplemented with 10% FBS, 1 mM sodium pyruvate (Euroclone), 0.1 mM non-essential amino acids (Euroclone).

Human-derived mostly diploid SUM159 cells (breast cancer, female), gene edited to express AP2σ2-EGFP and CLTA-TagRFP, were grown at 37°C and 5% CO_2 in DMEM/F12 supplemented with 5% fetal bovine serum (FBS; S11150; Atlanta Biologicals, Flowery Branch, GA), 100 U/ml penicillin and streptomycin (45000-652; VWR International, Radnor, PA), 1 μg/ml hydrocortisone (H4001; Sigma-Aldrich, St. Louis, MO), 5 μg/ml insulin (I9278; Sigma-Aldrich), and 10 mM 4-(2-hydroxyethyl)- 1-piperazineethanesulfonic acid (HEPES; 25-060-CI; Mediatech, Manassas, VA), pH 7.4.

AP2$\mu^{fl/fl}$ mouse embryonic fibroblasts (MEFs) were isolated from AP2$\mu^{fl/fl}$ mice (Kononenko et al., 2014) as previously described (Pozzi et al., 2012), and were spontaneously immortalized after a series of passages in cultures (information about sex of these cells is not available). AP2$\mu^{fl/fl}$ MEFs were cultured at 37°C and 5% CO_2 in Dulbecco's Modified Eagle Medium (DMEM, Lonza) supplemented with 10% FBS and glutamine 2 mM. Immortalized AP2$\mu^{fl/fl}$ MEFs were infected with pMSCV retroviral vector expressing AP2σ2-EGFP and CLTA-TagRFP (Cocucci et al., 2012) and subjected to selection with puromycin for 7 days.

AP2-EGFR MEFs used in EM experiments (Figures 4C, 4D, and 5D) were generated by infecting AP2-WT MEFs with pSLIK-EGFR inducible lentiviral vector. Forty-eight hours after infection, selection of infected cells was performed by adding neomycin at a concentration of 400 μg/ml for seven days. To induce expression of the EGFR transgene, doxycycline (0.05 μg/ml) was added to cell culture medium for 16 hours.

Human cells were authenticated at each batch freezing by STR profiling (StemElite ID System, Promega). All cell lines were tested for mycoplasma at each batch freezing by PCR (Uphoff and Drexler, 2002) and biochemical assay (MycoAlert, Lonza).

METHOD DETAILS

EGF concentrations, constructs and antibodies

Throughout the manuscript, we have used a low EGF concentration (1.5 ng/ml), unless otherwise indicated.

Constructs

pMSCV retroviral vectors expressing AP2σ2-EGFP and CLTA-TagRFP were previously described (Cocucci et al., 2012); the pSLIK-EGFR vector was generated by subcloning the cDNA coding for human EGFR from a pBABE-based vector (Sigismund et al., 2005) to the pSLIK-neo lentiviral vector [for inducible expression in mammalian cells (Shin et al., 2006)].

Antibodies

rabbit polyclonal anti-EGFR (epitope: aa 1172-1186, *Homo sapiens*), mouse anti-eps15 (epitope: aa 2-330, *Mus musculus*), rabbit anti-eps15L1 (epitope: aa 216-266, *Mus musculus*), mouse anti-epsin1/2 (epitope: aa 249-401 of epsin1, *Homo sapiens*) were produced in-house and used in IB experiments. Mouse anti-EGFR 13A9 (Genentech) was used to follow endocytosis in *in vivo* EM analyses. Anti-Alexa Fluor 488 (ThermoFisher) was used for cryosection immunolabeling for EM analysis. Other antibodies used in IB are listed in the Key Resources Table.

CRE treatment of AP2$\mu^{fl/fl}$ MEFs

In order to induce the excision of the AP2 gene and the complete loss of AP2 protein expression, immortalized AP2$\mu^{fl/fl}$ MEFs were treated with TAT-CRE recombinase produced in-house to obtain AP2-KO MEFs. Briefly, cells at 50%–60% confluency were washed twice in PBS and treated with 100 μg/mL of TAT-CRE in medium without serum at 37°C. After 1 h incubation, 50 μM chloroquine was

added to the medium for an additional hour at 37°C. Cells were then washed twice in PBS and supplemented with normal culture medium. The TAT-CRE treatment was repeated after 3 days; this second round of treatment is recommended to increase the efficiency of recombination. Experiments were performed after 14 days from the first TAT-CRE treatment. The experiments of endocytosis with ^{125}I-EGF and ^{125}I-Tf were confirmed also in AP2$\mu^{fl/fl}$ primary MEFs treated or not with CRE, obtaining the same results as with immortalized MEFs.

Genome editing of SUM159 cells using the TALEN-based approach

Human-derived mostly diploid SUM159 cells were homozygously gene edited to express endogenous CLTA-TagRFP together with AP2σ2-EGFP using the TALEN protocol (Sanjana et al., 2012). The TALEN target sequences were located as follow (the AP2σ2 downstream sequence overlaps with the stop codon underlined):

	5′ - > 3′ targeting sequences	position relative to stop codon
CLTA	TCTCCCTCAAGCAGGCCCCG	−9
	GTGGGACACCTTTGTGATGT	+5
AP2σ2	TGGGGCTCGCCTGCCCTCAC	−14
	TGCTGAAACAGCTGCTGATG	0*

The cells were generated as described (He et al., 2017; Aguet et al., 2016). Briefly, SUM159 cells were co-transfected with the upstream and downstream TALEN targeting sequences and the donor construct coding for the fluorescent protein using TransIT-2020 Transfection Reagent (Mirus Bio LLC, Madison, WI). Cells expressing endogenous clathrin light chain A (CLTA gene) fused to TagRFP at its C terminus and endogenous σ2 of AP-2 (AP2S1 gene) fused at its C terminus with EGFP were sorted by flow cytometry single cell sorting. The insertion of the sequence coding for the fluorescent protein on both alleles was verified by PCR amplification from purified genomic DNA using GoTaq Polymerase (Promega, Madison, WI) using:

for the CLTA gene, forward 5′-TTGTTGTTGCTTCCAGGGCA-3′ and reverse 5′-GCCAGGGAGAACACAGTTGA-3′ primers
for the AP2S1 gene, forward 5′-TGAGGTCTGTGTCCCAGCTC-3′ and reverse 5′-GGTTACTCGGGACACACACG-3′ primers.

TIRF based live-cell microscopy imaging and analysis

The TIRF microscopy including cell plating was carried as described (Aguet et al., 2016; Cocucci et al., 2014; Cocucci et al., 2012) using conditions that would allow detection of the fluorescence intensity from a single molecule of EGFP within a diffraction limited spot.

SUM159 cells were plated onto glass coverslips for 3-4 h whereas MEF cells were plated onto the fibronectin-coated coverslips for 2-3 h, after which they were washed with sterile PBS, transferred onto an Attofluor Cell Chamber (Invitrogen) containing 800 μL of prewarmed MEMα without phenol red (GIBCO) supplemented with 5% FBS and then placed onto a temperature controlled sample holder (20/20 Technology, Wilmington) enclosed placed inside the environmentally controlled chamber of the microscope and time series acquired as described (Aguet et al., 2016; Cocucci et al., 2014; Cocucci et al., 2012).

Time series obtained using TIRF microscopy were analyzed using the cmeAnalysis software package (Aguet et al., 2013) to trace clathrin-coated structures labeled with CLTA-TagRFP (master channel) and classified as those either containing AP2-σ2-EGFP for at least 40% of their lifetimes (AP2+) or those lacking AP2-σ2-EGFP (AP2-). A range of initial mean squared displacement (MSD) cutoffs (0.010, 0.0155 or 0.02 μm^2), calculated from the sum of the squares of displacement in x and y between the first and second time points, were used to differentiate relatively immobile clathrin structures initiating at the plasma membrane from those potentially originating at the trans-Golgi network or endosomes. The relatively immobile clathrin traces were then grouped according to their content of AP2 grouped by lifetimes.

RNAi experiments

For eps15/eps15L1 double KD, HeLa cells stably depleted using pSICOR-shRNA sequences directed against human eps15 and eps15 L1 were previously described (Sigismund et al., 2005). These cells were subjected to transient RNAi-mediated knockdown for epsin1, epsin2, clathrin or AP2 in different combinations, as indicated.

RNAi transfections were performed using LipofectAMINE RNAi MAX reagent from Invitrogen, according to manufacturer's instructions. Cells were subjected to double transfection (in both suspension and adhesion), treated with 10 nM RNAi oligo (except for clathrin KD: 24 nM RNAi oligo). Cells were analyzed 4-5 days after transfection.

RNAi oligos

The negative control siRNA used in our assays was All Stars from QIAGEN. Other oligos were indicated in the Key Resources Table.

Quantitative real-time PCR analysis

Total RNA was extracted from HeLa and MEF cells (control, KD or KO, as indicated) using the RNeasy kit from QIAGEN, according to the manufacturer's protocol. Single stranded cDNA synthesis was performed using the QuantiTect Reverse Transcription Kit (QIAGEN) following manufacturer's instructions.

For the analysis of KD levels by RT-qPCR, the Taqman chemistry (Thermo Fisher Scientific) was used; qPCR instrument was from Applied Biosystems. For the different genes, inventoried Taqman assays (Applied Biosystems) were employed, indicated in the Key Resources Table.

For the transcriptomics analysis of EGF-induced genes (Figures 7A and 7B), total RNA was reverse-transcribed with SuperScript® VILO cDNA Synthesis Kit (Life Technologies cat.no. 11754050) and measured with Quantifast SYBR green master mix (QIAGEN) in Biorad Cfx384 RT-qPCR detection system. The complete list of primers used in this study is shown in Table S1.

Cell lysis and immunoblot (IB)

Cells were lysed in RIPA buffer (50 mM Tris–HCl, 150 mM NaCl, 1 mM EDTA, 1% Triton X-100, 1% sodium deoxycholate, 0.1% SDS); protease inhibitor cocktail (CALBIOCHEM) and phosphatase inhibitors (20 mM sodium pyrophosphate pH 7.5, 50 mM NaF, 2 mM PMSF, 10 mM Na3VO4 pH 7.5) were freshly added.

For EGF stimulation, HeLa or MEF cells were plated on five 10 cm dishes at 50% confluence. The day after, cells were serum starved for 16 h and then stimulated at the indicated time points with 1.5 ng/ml EGF. Total cell lysates (20-30 μg) were loaded onto 4%–20% gradient precast SDS polyacrylamide gels (BIORAD). IB and IP were performed as described (Conte and Sigismund, 2017; Penengo et al., 2006).

Radioactive assays

Surface EGFRs were measured by ^{125}I-EGF saturation binding as described (Sigismund et al., 2013). Radioactive internalization assays were performed as described (Caldieri et al., 2017) with 1.5 ng/ml of ^{125}I-EGF or 1 μg/ml of ^{125}I-Tf. Results are expressed as the internalization rate constant [Ke, (Caldieri et al., 2017)] or as a % of Ke in control cells, as indicated, and are the mean ± SD, calculated on duplicate points of at least two independent experiments.

Degradation of ^{125}I-EGF at low dose was measured as described (Sigismund et al., 2008). In brief, HeLa cells, subjected to KD as indicated, were serum-starved for 2 hours and then incubated with 1.5 ng/ml ^{125}I-EGF for 8 min at 37°C, followed by mild acid/salt treatment (0.2 M Na Acetate buffer pH 4.5, 0.5 M NaCl) for 5 min at 4°C to remove bound EGF. ^{125}I-EGF-loaded cells were then chased in medium without serum at 37°C for the indicated time points. At the end of each chase time, the medium was collected, the surface-bound ^{125}I-EGF was extracted by acid treatment (0.2 M acetic acid pH 2.8, 0.5 M NaCl), and the cells were lysed in 1 mM NaOH. The medium and intracellular lysate fractions were then TCA-precipitated to separate intact from degraded ^{125}I-EGF. Non-specific counts were measured for each time point in the presence of a 300-fold excess of cold ligand, and were never > 3%–10% of the total counts.

Cell migration assay

Cell migration assays were performed using a BD Boyden Chamber (BD Biosciences) with 8 μm pores, coated with Collagen I rat tail (10 μg/ml, BD Biosciences). Both chambers were filled with medium. The lower chamber contained serum-starved medium, EGF (1.5 ng/ml) or complete medium. Serum-starved cells (4x10^4 cells/well) were seeded into the upper chamber of the transwell and allowed to migrate overnight at 37°C. Three replicates for each condition were performed. After the incubation period, cells remaining in the upper chamber were washed away with PBS and removed by a cotton swab. Fixed cells were then stained with DAPI. Cells were counted in three randomly chosen fields using an inverted fluorescence microscope (10X magnification).

Plasma membrane sheets (PMS)

PMS were prepared as previously described (Sanan and Anderson, 1991). Briefly, formvar/carbon coated nickel grids coated with 1 mg/ml poly-Lysine-D were placed on a pre-wet filter of cellulose acetate on ice. Cells were washed with KSHM buffer (100 mM potassium acetate, 85 mM sucrose, 20 mM HEPES-KOH, pH 7.4, and 1 mM magnesium acetate) and the coverslips were placed cells face down on the EM grids. The excess of buffer was aspirated with a pasture pipette attached to a vacuum pump and a rubber cork was pressed on the coverslip for 10 s. The coverslips were flipped over and the grids were fixed on ice for 30 min in 4% glutaraldehyde in KSHM buffer. PMS were then post-fixed in 1% OsO4 10 s on ice, 1% tannic acid, 1% uranyl acetate and finally rinsed in distilled water and air-dried.

Grids were observed with a LEO 912AB Zeiss Transmission Electron Microscope (Carl Zeiss). Digital micrographs were taken with a 2k × 2k bottom-mounted slow-scan Proscan camera (ProScan) controlled by the EsivisionPro 3.2 software (Soft Imaging System) and analyzed using ImageJ as previously reported (Grove et al., 2014).

Transmission Electron Microscopy (TEM)

For TEM analysis, cells treated as indicated were fixed for 1 h at room temperature in 2,5% glutaraldehyde in 100 mM NaCacodylate buffer pH 7.2 and then post-fixed in 1% osmium tetroxide, 1,5% potassium ferricyanide in 100 mM NaCacodylate buffer for 1 hour on

ice. Alternatively, in order to discriminate plasma membrane connected pits, cells were fixed with 1.25% glutaraldehyde in 66 mM NaCacodylate buffer containing 0.5mg/ml ruthenium red. After several washes in 150 mM NaCacodylate buffer cells were post fixed in 1.3% osmium tetroxide in a 66 mM NaCacodylate buffer (pH 7.2) containing 0.5 mg/ml ruthenium red for 2 h at room temperature. Both samples were then rinsed in NaCacodylate buffer, washed with distilled water and enbloc stained with 0.5% uranyl acetate in dH_20 overnight at 4°C in the dark. Finally, samples were rinsed in dH_2O, dehydrated with increasing concentrations of ethanol, embedded in Epon and cured in an oven at 60°C for 48 h. Ultrathin sections (70 – 90 nm) were obtained using an ultramicrotome (UC7, Leica microsystem, Vienna, Austria), collected, stained with uranyl acetate and Sato's lead solutions, and observed in a Transmission Electron Microscope (Leo 912AB, Carl Zeiss, Oberkochen, Germany). Digital micrographs were taken with a 2Kx2K bottom mounted slow-scan camera (ProScan, Lagerlechfeld, Germany) controlled by the EsivisionPro 3.2 software (Soft Imaging System, Münster, Germany). For Morphometrical analysis images of the random selected cellular profiles were analyzed using ImageJ software. CCP density was calculated by dividing the number of CCP for PM length, and further normalized for the variation in cell size observed.

Pre-embedding immunolabeling

Serum-starved cells were incubated with anti-EGFR 13A9 antibody, followed by incubation with rabbit anti-mouse, and, finally, with Protein A-gold 10 nm (Utrecht University), 30 min incubation on ice/each step. Cells were then incubated at 37°C for 5 min with 30 ng/ml EGF. A control sample incubated with all reagents except anti-EGFR 13A9 antibody was included in the experiment to control that no internalization was induced by the secondary antibody and Protein A-gold 10 nm (Figure S3F). Cells were then washed in PBS and fixed for 1 h at room temperature in 1.2% glutaraldehyde in 66 mM sodium cacodylate buffer pH 7.2 containing 0.5 mg/ml of ruthenium red. After quick washes with 150 mM sodium cacodylate buffer, the samples were post-fixed in 1.3% osmium tetroxide in a 66 mM sodium cacodylate buffer (pH 7.2) containing 0.5 mg/ml ruthenium red for 2 h at room temperature. Cells were then rinsed with 150 mM NaCacodylate, washed with distilled water and enbloc stained with 0.5% uranyl acetate in dH20 overnight at 4°C in the dark. Finally, samples were rinsed in dH2O, dehydrated with increasing concentrations of ethanol, embedded in Epon and cured in an oven at 60°C for 48 h.

Anti-EGF immunolabeling of cryosections

As an independent procedure to visualize EGFR internalizing clathrin-coated pits (CCPs), we performed cryosection experiments (Figures S3F and S3G). Briefly, cells were stimulated with Alexa 488 EGF (30 ng/ml) for 5 min, fixed for 1 h at room temperature (0.2% glutaraldehyde/ 2% paraformaldehyde in PHEM Buffer 0.1 M) and processed as described previously (Slot and Geuze, 2007). Briefly, samples were embedded in 12% gelatin, infiltrated in 2.3 M sucrose and frozen in liquid nitrogen. Cryosections were obtained using a Leica EM FC7 ultramicrotome (Leica microsystem, Vienna, Austria) and collected on 150 mesh formvar carbon-coated copper grids. The labeling procedure was carried out using a rabbit anti-Alexa Fluor 488 antibody (5 μg/ml) in 1% BSA in PBS that was afterward visualized with proteinA conjugated to 10 nm colloidal gold particles (Protein A-gold 10 nm, Utrecht University). Grids were contrasted in a solution of uranyl acetate and methyl-cellulose, air-dried and observed in a Talos L120C transmission electron microscope (Thermo Fisher Scientific).

Analysis of cell surface area and perimeter

Cells grown on coverslips were fixed and stained with phalloidin-FITC. Nuclei were counterstained with DAPI. Fluorescence imaging was performed with a Confocal Leica TCS SP5 using a 40X 1.40 NA oil objective and LAS software. Z stacks of different cells were collected. Images were analyzed using ImageJ software. Single cells were selected with ROIs (region of interest) and geometrical properties of each cell (perimeter, basal area, thickness as well as major and minor axis of the best fitting ellipse) were determined. Selected cells were approximated to elliptic cones shape and the total surface area calculated. Per each sample 50 cells were analyzed.

QUANTIFICATION AND STATISTICAL ANALYSIS

For radioactive assays, statistical analysis was performed using two-tailed Student's t test with Excel when we compared two conditions. When more conditions were compared, Each Pair Student's t test with JMP 10.0 statistical software (SAS Institute, Inc) was performed, which exploits the Fishers LSD test as a follow up to ANOVA.

Quantitation of the blots was performed with Photoshop. Statistical analysis was performed using two-tailed Student's t test with Excel.

For migration assay, statistical analysis was performed using two-tailed Student's t test with Excel.

For PMS and TEM, images were analyzed with ImageJ and statistical analysis was performed using GraphPad Prism. Two tailed paired Student's t test was used to calculate statistical significance among different samples.